Mechanical and Electromechanical Properties of Graphene and their Potential Applications in MEMS

Zulfiqar H. Khan,[1] Atieh R. Kermany,[1] Andreas Öchsner,[2] Francesca Iacopi[1,*]
[1]Environmental Futures Research Institute, Griffith University, Nathan, Queensland 4111, Australia;
[2]School of Engineering, Griffith University, Gold Coast, Queensland 4125
[*]*presently at School of Computing and Communications, University of Technology Sydney, Broadway NSW 2007, Australia, email: francesca.iacopi@uts.edu.au*

Contents

Keywords: MEMS, Graphene, Mechanical Property, Thermo-Mechanical Property, Electromechanical Properties, Adhesion, Tribology, Piezoresistivity, Piezoelectricity, Resonator, Sensor.

Abstract:

Graphene-based microelectromechanical systems (MEMS) are very promising candidates for next generation miniaturised, lightweight, and ultra-sensitive devices. In this paper we review the progress to-date of the assessment of the mechanical, electromechanical, thermomechanical properties of graphene towards application in graphene-based MEMS. Graphene possesses a plethora of outstanding properties—such as a 1 TPa Young's modulus, exceptionally high 2D failure strength that stems from its sp^2 hybridization, and strong sigma bonding between carbon atoms. Such exceptional mechanical properties can enable, for example, graphene-based sound sources capable of generating sound beyond the audible range. The recently engineered piezoelectric properties of AFM-tip-pressed graphene membranes or supported graphene on SiO_2 substrates, have paved the way in fabricating graphene-based nanogenerators and actuators. On the other hand, graphene's piezoresistive properties have enabled miniaturized pressure and strain sensors. Two-dimensional graphene nanomechanical resonators can potentially measure

ultralow forces, charges and potentially detect single atomic masses. The exceptional tribology of graphene can play a significant role in achieving superlubricity. In addition, the highest reported thermal conductivity of graphene is amenable for use in chips and providing better performing MEMS, as heat is efficiently dissipated. On top of that, graphene membranes could be nanoperforated to realize specialized applications like DNA translocation and desalination. Finally, to ensure stability and reliability of the graphene-based MEMS, adhesion is an important mechanical property that should be considered. In general, graphene could be used as a structural material in resonators, sensors, actuators and nanogenerators with better performance and sensitivity than conventional MEMS.

1. Introduction

Graphene, an allotrope of carbon, is a single atomic layer of graphite made up of very tightly bonded carbon atoms with a carbon–carbon bond length of 0.142 nm and sp^2 hybridization organised into a hexagonal lattice in 2D. In 2004, Geim and Novoselov exfoliated and transferred monolayer graphene from bulk graphite onto thin SiO_2 on a silicon wafer using the Scotch tape technique [1]. As a result of this study, they won the 2010 Nobel Prize in Physics [2].

In this review, we will focus on the mechanical-related properties of graphene. The origin of these exceptional properties is linked to sp^2 hybridization and sigma bonding, which is the strongest covalent bond [3]. Graphene was reported to have a very high Young's modulus of 1 TPa [4, 5]. In addition, defect-free graphene's failure strength is 42 N/m, [4] 100 times stronger than the strongest steel [2, 6]. Also, graphene shows exceptional experimental ductility: it is up to 20% stretchable [7, 8]. Graphene could be used to produce transparent electrodes [9]; ultra strong and tough composites [10, 11]; and ultra-thin, flexible [12, 13], stretchable [13] display or touch-screens and energy storage applications [14, 15].

Among the various electromechanical coupling methods, the piezoelectric transduction is the most common and most frequently used method for conventional MEMS. Until recently, piezoelectric transduction could not be applied to graphene MEMS because intrinsic graphene is symmetric in nature and therefore does not show piezoelectric properties. The piezoelectric properties of graphene have been recently engineered, which paves the way for future dynamic control of graphene-based MEMS/NEMS devices and opens up new possibilities for energy

harvesting, actuation, and transduction [8, 16]. On the other hand, using the piezoresistive effect, graphene offers opportunities to replace currently available commercial MEMS pressure [17] and strain [18] sensors. The sensitivity per unit area of a graphene-based pressure sensing device is an order of magnitude higher than that of conventional devices [19]. In addition, the large exposed surface area with ultralow mass and high Young's modulus makes graphene nanomechanical resonators suitable for high resolution mass sensing [20]. Moreover, these resonators could be used as ultralow force and charge sensors [20], and as thermo-sensors [21]. Monolayer graphene was found to have thermal conductivity as high as 5000 W/mK at room temparature [22, 23]. Thus, graphene could be used as a thermal management material because it conducts heat away and prevents overheating [24]. Another interesting property of graphene is its negative coefficient of thermal expansion (CTE) below a critical temperature [25].

The adhesion energy of graphene with substrate is an important mechanical property for the wafer- level production of micro- and nano-devices because high adhesion ensures manufacturability and stability of operation over a long period [26]. Thus, adhesion of both transferred and transfer-free graphene with the substrate should be investigated. On top of that, tribology will be investigated since the exceptional tribology of graphene makes it useful for reducing friction between tribo pairs, using as a solid lubricant, protecting metal from corrosion, and providing a protective coating. In this review, we intend to highlight graphene's nano-scale and macro-scale friction and wear properties.

2. Brief Review of the Types of Graphene

For replacing currently available commercial MEMS to realize graphene based devices on a large scale, the quality of graphene and the cost of the graphene production are of paramount importance. Moreover, researchers have to produce large sheets of graphene of ultimate purity and large domain size; with minimum defects or structural disorders; and of uniform thickness, with control of the thickness as needed. In addition, graphene should be available in a suitable form, at the required quantity, and of desirable thickness, according to individual application requirements, and there should be an appropriate control of these factors in the graphene production process.

In order to meet these challenges, several promising graphene synthesis techniques have been reported such as chemical vapor deposition (CVD) onto transition metal foil [9, 27, 28];

mechanical/liquid phase/thermal exfoliation [1, 29]; chemical reduction of graphite oxide (GO); and epitaxial graphene (EG) [30, 31] on SiC.

CVD graphene is promising in making flexible and transparent electronics [12, 32-35] and corrosion protective coatings [36-40]. However, the transfer of the CVD graphene to an appropriate substrate is the main drawback for using CVD graphene at the wafer level.

When purity and quality of graphene is not the major issue, then the exfoliation (mechanical/thermal/liquid phase) and reduction of GO are the most suitable methods for producing large quantities of graphene at low cost. For example, in conductive coatings and inks [41-44], fuel cells [45], and lithium batteries [46-48], exfoliated graphene could be efficiently used.

In general, graphene production can be categorized into two types: transferred graphene and transfer-free graphene. The CVD growth on metal foil [49-51], the reduction of GO and the exfoliation technique can be generalized as transferred graphene, since the transfer of the graphene onto an appropriate substrate is needed for device fabrication. On the other hand, epitaxial graphene is transfer-free graphene as it is grown on a wide bandgap semiconductor substrate (SiC) without the need for transfer [52]. This transfer-free epitaxial graphene on SiC is a potential method for future wafer level production of graphene based devices [53]. The main limitation of epitaxial graphene is the high cost of SiC and the requirement of elevated temperatures for its production [54].

Table 1. Overview of different methods for production of graphene

Method	How to Produce	Advantages	Disadvantages	Application
Micromechanical exfoliation	Layers of graphite are peeled off by using Scotch tape and repeated peeling results in graphene.	Does not need high-tech instruments; high quality graphene	Not scalable	Lab-based experiments
Liquid phase and thermal exfoliation	Using chemical solvents or thermal shock, graphene flakes are produced from graphite.		The number of layers is hard to control, the process can introduce impurities.	Batteries of the fuel cells, inks, conductive coatings.
Chemical reduction of graphene oxide	Graphene oxide is ultrasonically/thermally exfoliated in an aqueous solution, processed by centrifugation, deposited as a thin film on substrate and reduced to graphene.	Scalable to large-scale production		
Chemical vapour deposition (CVD)	Carbon-containing gases (e.g. CH_4, C_2H_6) decompose on a transition metal (e.g. Cu, Ni) surface at high temperature (700-1000^{0}C) and turn into graphene.	Scalable High quality Low cost Good control	Complex transfer process	Flexible, transparent electrode/electronics, sensors, coating
Thermal decomposition of SiC	Evaporation of Si takes place at high temperature (>1200^{0}C); annealing causes the evaporation of Si and a graphene layer is formed.	Scalable, High quality No transfer required Good control over the process	High cost of silicon carbide	Sensors, current CMOS technology

3. Mechanical Properties of Graphene

3.1. Elastic and Fracture Properties

Graphene has exceptional elastic properties; the strength, elasticity and intrinsic stress of graphene were measured by both theoretical modelling [55, 56] and lab-based experiments [4, 57]. Because graphene is a nanoscale material, most of the physical attributes are different from those of bulk graphite.

As the monolayer graphene is two-dimensional in structure, its elastic properties are described by a two-dimensional stress (σ^{2D}), second order elastic stiffness, or Young's modulus (E^{2D}) and third order elastic modulus (D^{2D}). If ε is the uniaxial Lagrangian strain, then the symmetric second Piola-Kirchhoff stress is given by [4, 58],

$$\sigma^{2D} = E^{2D}\varepsilon + D^{2D}(\varepsilon)^2 \quad (1)$$

and the intrinsic stress is given by, $\sigma_{\text{int}} = -E^2/4D$ (2)

at the strain $\varepsilon_{\text{int}} = -E/2D$ (3)

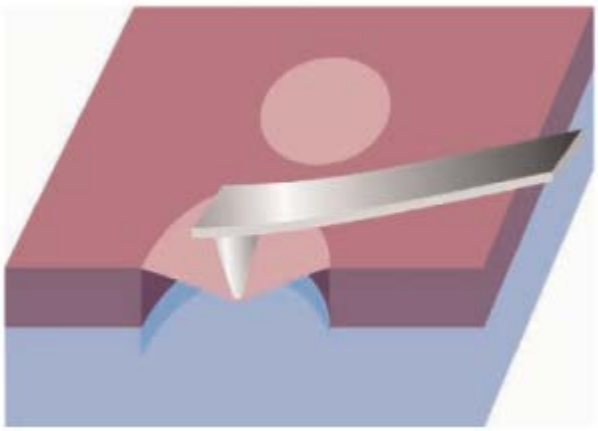

Figure 1. AFM nanoindentation to evaluate mechanical properties (adapted from Ref. [59])

Some exceptional elastic properties of a defect-free, suspended single layer of mechanically exfoliated graphene which was clamped by small circular (~ 1 to 1.5 μm diameter) holes, were measured by Lee *et al.* [4] by means of atomic force microscope nanoindentation. For monolayer graphene, E^{2D} = 340 $\pm$ 50 N/m and D^{2D} = - 690 $\pm$ 120 N/m. According to Lee *et al.*, if the thickness of graphene is taken as 0.335 nm, then the Young's modulus (*E*) becomes 1.0 ± 0.1

TPa (which is similar to that of graphite) and the third-order elastic stiffness (D) becomes –2.0 ± 0.4 TPa with intrinsic stress σ_{int} = 130 ± 10 GPa at a strain of ε_{int} = 0.25 [4]. In another study, Lee and his co-workers [57] applied a pressure difference on a clamped circular monolayer exfoliated graphene membrane. They used the Raman G-peak shift to measure strain in graphene membranes, then compared the measured strain to the numerical simulation, and reported a Young's modulus of 2.4±0.04 TPa.

Lee and his co-workers [4] measured the 2D failure strength or intrinsic strength of graphene as 42 N/m by nanoindentation with an atomic force microscope. A hypothetical steel film of the same thickness as graphene would give a 2D failure strength of 0.084-0.40 N/m, which proves that defect free graphene is more than 100 times stronger than the strongest steel and can be considered as the strongest material [2]. On the other hand, nanoindentation measurements suggest that the breaking stress at the grain boundaries of CVD graphene is ~35 GPa or less [60]. In graphene, hexagonal unit cells contain two carbon atoms with an area of 0.052 nm^2, thereby giving the calculated density of graphene as 0.77 mg/m^2. A hypothetical graphene-made hammock weighing 0.77 mg can cover 1 m^2 area and support 4 kg weight [2]. Moreover, graphene can theoretically sustain up to 25% in-plane tensile elastic strain [61, 62] whereas 20% of stretch has been demonstrated experimentally so far [7, 8]. Note that the mechanical properties in this section have been measured at room temperature.

The heat generation in graphene-based devices causes an increase in temperatures, which causes detrimental effects on the mechanical properties of graphene. For example, Zhang *et al.* [63] theoretically showed that increasing temperature leads to a linear decrease of Young's modulus.

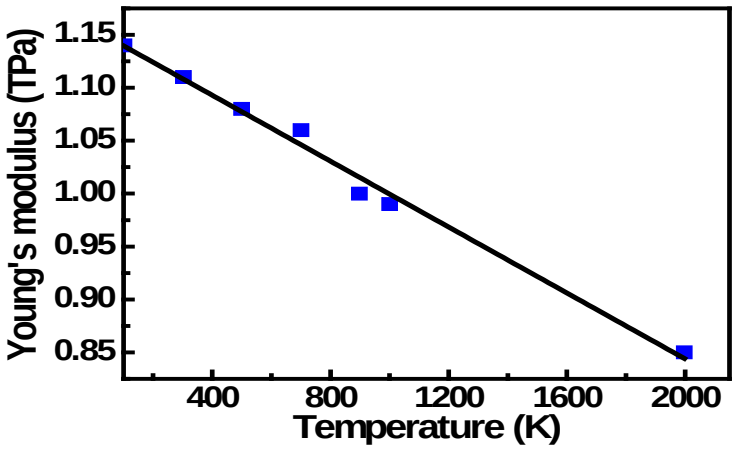

Figure 2. Change of Young's modulus as a function of temperature (adapted from Ref. [63])

3.2. Thermo-Mechanical Properties

Thermal management is one of the most important challenges for micro and nano devices. As graphene exhibits excellent thermal conductivity, it will efficiently remove heat from circuit hot spots, to heat sinks [64]. Balandin *et al.* [22] reported an extremely high thermal conductivity of defect-free monolayer suspended graphene, which ranges from 4840 to 5300 W/mK at room temperature. To extract the value of thermal conductivity, the temperature rise with respect to laser power was determined from the G peak shift of a suspended graphene layer using confocal micro-Raman spectroscopy, while heat propagated transversely towards the graphitic heat sinks. The thermal conductivity of suspended graphene exceeds that of a single-walled carbon nanotube (3500 W/mK) [65]; multi-walled CNT (3000 W/mK) [66]; diamond (1000–2200 W/mK) [22]; and graphite (1910 W/mK [67]). On the other hand, exfoliated monolayer graphene supported on a silicon dioxide substrate shows a thermal conductivity of about 600 W/mK near room temperature, still higher than those of metals [68]. The thermal conductivity is affected by isotopic doping; for example, isotopically pure ^{12}C (with only 0.01% ^{13}C) graphene demonstrates a higher value of thermal conductivity than any other percentage combination of ^{12}C and ^{13}C [69].

Using atomistic simulations based on an accurate interatomic potential for carbon, Los *el al.* [70] estimated the melting temperature of graphene, T_m = 4510 K. Los *et al.* proposed that the melting of graphene is a two step process, namely, 2D solid → quasi-2D liquid → 3D liquid, where the first step follows a first order transition [70]. Zakharchenko *et al.* [71] found that clustering of Stone–Wales defects and formation of octagons leads to a liquid of entangled carbon chains, and thus melting of graphene occurs.

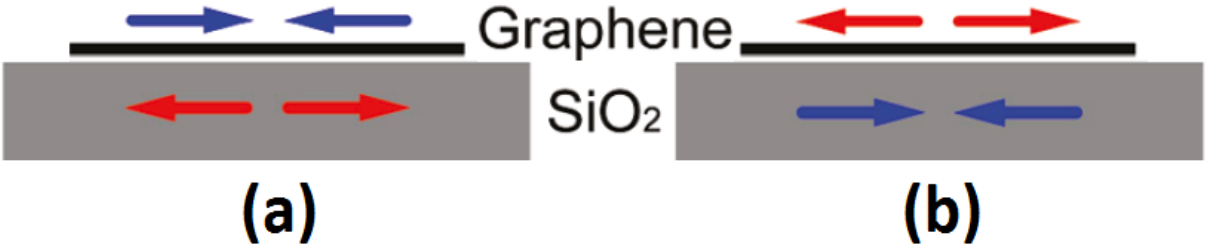

Figure 3. a) Heating process and b) Cooling process (adapted from Ref. [25])

The coefficient of thermal expansion (CTE) for graphene is negative [25], whereas it is positive for most of the substrates, for example, Si, SiC, SiO_2 and so on. As a result, when heat is

applied, contraction of graphene and elongation of substrate (e.g. SiO_2) take place simultaneously (figure 3a). During the cooling process, expansion of graphene simultaneously occurs with contraction of SiO_2, that is, the opposite phenomenon takes place (figure 3b).

A precise and accurate description of the CTE over a wide range of temperatures is essential to fabricate graphene-based devices. Several authors have calculated or measured the CTE of monolayer graphene using various experimental methods and theoretical simulations.

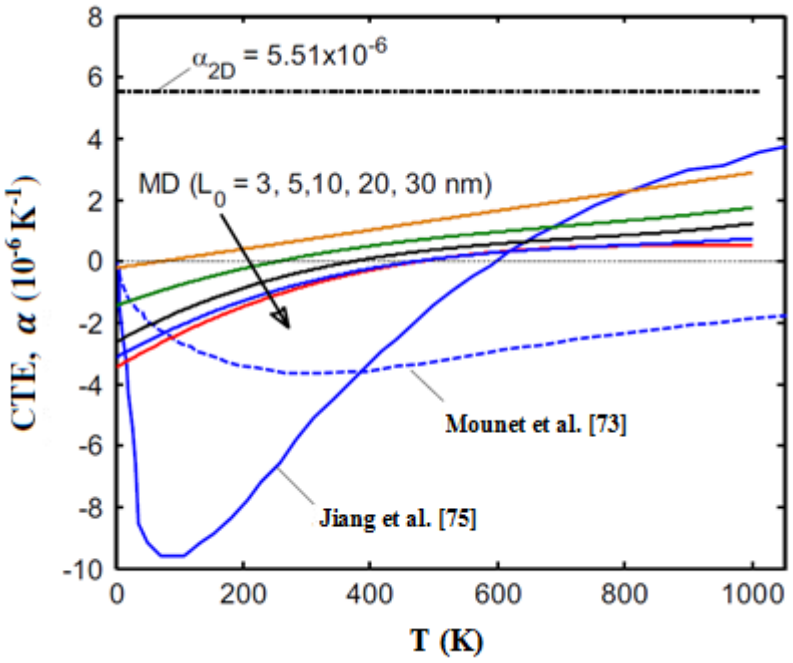

Figure 4. CTE of graphene vs. Temperature; a comparison of different studies (adapted from Ref. [72])

From ab initio density functional theory (DFT) calculations and a quasiharmonic approximation (QHA), Mounet *et al.* [73] demonstrated a negative coefficient of thermal expansion for graphene with the help of Grüneisen parameters. Note that positive Grüneisen parameters correspond to positive CTE and negative Grüneisen parameters are associated with negative CTE.

Grüneisen parameters are defined by the following equation [73]:

$$\gamma_j(q) = -\left[\frac{a}{2\omega_j(q)}\right]\left[\frac{d\omega_j(q)}{da}\right], \qquad (4)$$

where q stands for wave vector and $2\omega_j(q)$ represents the frequency of the j^{th} mode of a phonon in the Brillouin zone.

The substrate materials, such as silicon or silicon carbide, demonstrate positive Grüneisen parameters only. However, the theoretical study by Mounet *et al.* [73] demonstrated that, in graphene, negative Grüneisen parameters associated with out of plane acoustic bending modes could be easily excited (figure 5). The dominance of the phonon modes associated with these negative Grüneisen parameters give rise to the negative CTE of graphene.

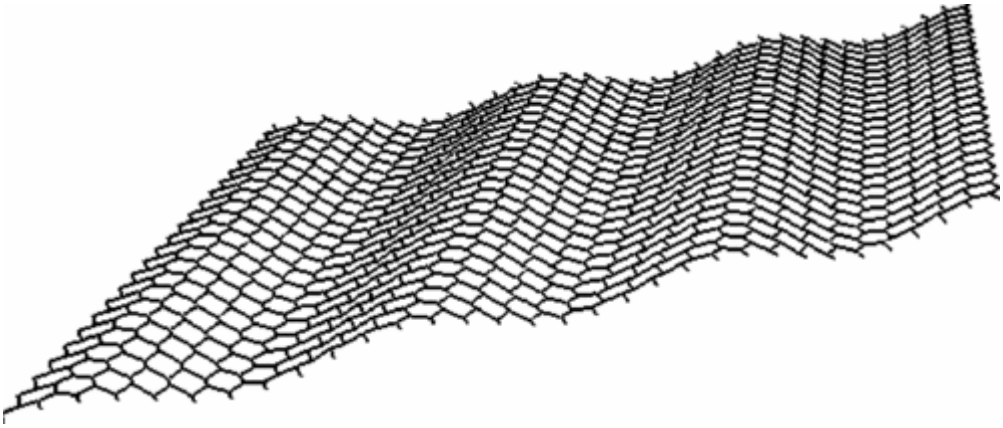

Figure 5. Bending mode of a graphene sheet which is responsible for negative CTE (adapted from Ref. [73])

Table 2. Summary of the CTE of graphene by different methods

TEC (K^{-1})	Method	Author
-8 x 10^{-6}	Raman spectroscopy	Yoon *et al.* [25]
$-7x10^{-6}$	Frequency of suspended graphene electromechanical resonators	Singh *et al.* [74]
$-6x10^{-6}$	Nonequilibrium Green's function approach	Jiang *et al.* [75]
$-7x10^{-6}$	With SEM image of graphene membrane	Bao *et al.* [76]
~-3.7 x 10^{-6}	DFT calculations	Mounet *et al.* [73]

Unlike both quasiharmonic approximation (QHA) [73] and Green's function method [75], molecular dynamics (MD) simulations [72] demonstrated a monotonic increase of CTE of graphene with temperature (figure 4). The main reasons for the inaccuracy of classical MD simulations at low temperatures (T< 100 K) are the quantum effect and difficulty in predicting small dimension change.

With Raman spectroscopy, Yoon *et al.* [25] measured the CTE for monolayer graphene, which was found to be a function of temperature, and is negative for temperatures between 200 K and 400 K (e.g. -8×10^{-6} K^{-1} at room temperature). Using scanning electron microscopy, Bao *et al.* [76] observed a transition from a negative to positive CTE for suspended graphene between 300 K and 400 K. From the resonance frequency shift with a temparature change of suspended graphene electromechanical resonators, Singh *et al.* [74] reported a negative CTE ($\alpha < 0$) for the temperature range 30 K <*T*< 300 K. In conclusion, there is significant difference in experimental and theoretical values of the CTE of graphene (Figure 4). Note that for the temperature range 0 K<*T*< 700 K, graphite also shows a negative CTE [77].

Jiang *et al.* [75] used a nonequilibrium Green's function approach to measure CTE. The striking feature they found was that the CTE is very sensitive to the substrate-graphene interaction. Jiang *et al.* [75] also demonstrated that if the substrate-graphene interaction is ~0.06% of the in-plane interaction, then the negative TEC region of graphene is significantly reduced. Moreover, a strong interaction of graphene and the substrate leads to positive CTE for any temperature.

Due to thermal expansion mismatch of graphene and the substrate (figure 3), thermal stress is created when the temperature changes. The tensile thermal stress suppresses the thermal rippling, but compressive thermal stress favours thermal rippling of graphene on the substrate [76]. Thus temperature-dependent rippling amplitude could be attributed to the stress created from thermal expansion mismatch [78].

3.3. Tribology

The tribology of graphene includes the study of its wear and lubrication properties and of its frictional force and mechanisms at the micro- and nano-scale. The factors that play crucial roles in determining the friction of graphene are the graphene growth technique, structural defects, number of layers [59, 79], chemical functionalization [80, 81], substrate material [82] etc, among others. Moreover, some extrinsic factors such as environment (e.g. temperature, humidity), scan speed [83], applied load [84], tip geometry (e.g. size, shape) and composition can also affect the friction measurement and they need to be kept constant for a comparative study of friction [59, 85]. In addition to nano-scale friction tests performed by friction force microscopy (FFM), there are several reports of micro-scale friction tests [86]. Nanoscale friction, F_f is proportional to the real contact area, *A*.

$$F_f = \tau A, \quad (5)$$

where τ is a proportionality constant that represents the shear force per unit area [80, 87, 88] . The real contact area increases when the applied normal force between the tip and sample increases [87].

In order to measure nanoscale friction, a normal force needs to be applied to make AFM/FFM tip-graphene contact. After that, a lateral force needs to be applied by tilting the tip, and then the stick−slip motion of the tip needs to be measured [81]. While the counter tip is moved back and forth in one cycle, the difference between the lateral forces divided by two gives an estimate of friction forces [89, 90]. For explaining the nanoscale friction of graphene, two proposed mechanisms are possible: electron–phonon coupling [91], and the puckering effect [84, 89].

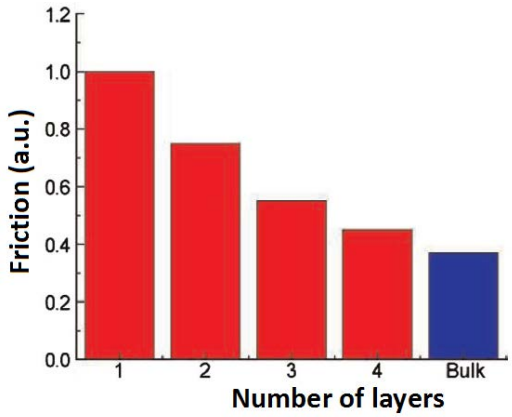

Figure 6. Friction vs. number of layers of graphene (adapted from Ref. [59])

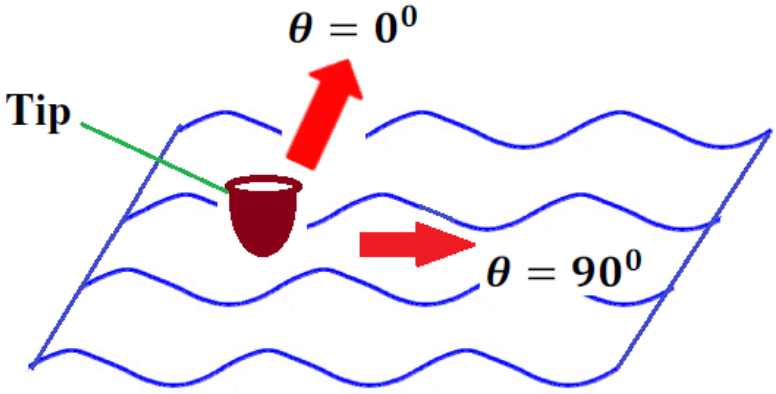

Figure 7. A schematic showing the puckering effect in an individual domain (redrawn from Ref. [84])

The nanoscale and microscale friction of graphene depends on the adhesion of graphene with the underlying substrate and on the number of graphene layers. The frictional force between a silicon tip of AFM and mechanically exfoliated graphene decreases monotonically with an

increase in the number of layers; above four layers, the frictional force approaches that of bulk graphite [59, 79]. Li *et al* [79] demonstrated that this trend applies only if the adhesion between graphene and its substrate is low. In that case, the bending stiffness is lower than the in-plane stiffness and thus the AFM tip/graphene top surface adhesion leads to out-of-plane deformation, which is also known as puckering [79, 89]. The final result of puckering is an increase in friction through the increase of contact area or additional work done [89]. As the number of layers decreases and a graphene sheet becomes thinner, its bending stiffness decreases and thus the puckering effect becomes more prominent [79, 89]. Moreover, Choi *et al.* [84] reported that a mechanically exfoliated monolayer graphene surface supported on the SiO_2 substrate, has domain structures that have different friction properties. In each domain, the ripples induce the puckering effect, which causes significant friction anisotropy with an angular periodicity of 180° on each friction domain. On the other hand, for strongly adhered graphene samples (e.g. graphene on mica), the puckering effect is suppressed, and thus friction is independent of the number of layers of graphene [79, 92].

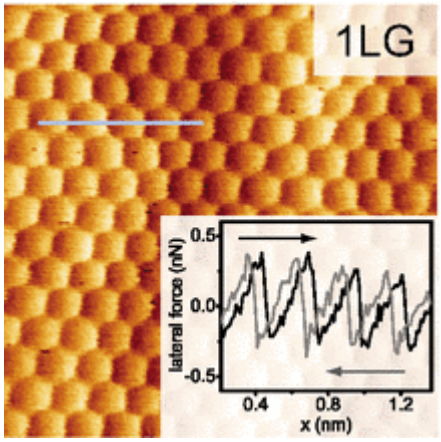

Figure 8. Map of lateral force and line profiles on monolayer graphene obtained by using a silicon tip having 13 nN normal load and 20 nm/s scan speed (adapted from Ref. [93])

Filleter *et al.* [93] observed periodic hexagonal stick-slip patterns with the same orientation for both single and two-layer graphene films on SiC(0001) which was grown by thermal decomposition. The sawtooth-shaped lateral force acts on the tip of the friction force microscope (FFM). However, below a critical load value, the stick-slip pattern and sawtooth lateral force disappear and smooth sliding begins [93].

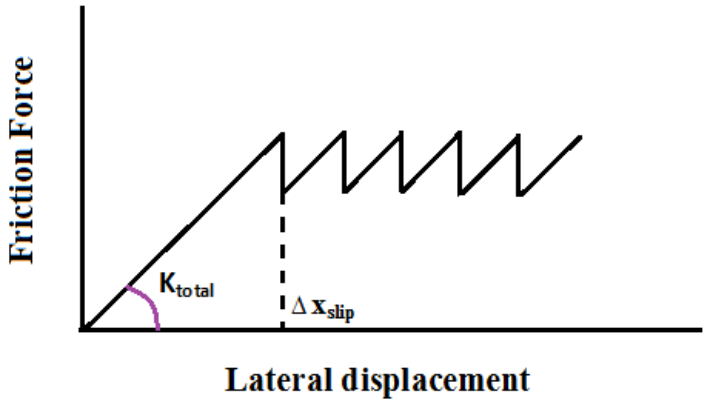

Figure 9. Schematic stick–slip friction profile (adapted from Ref. [87])

In an atomic stick-slip friction profile, each segment has a sloped part, stick, followed by a sharp decrease in the friction force, slip [89, 94]. For the stick–slip friction profile (figure 9) the measured friction force is represented as [87]

$$F_f = k_{total}.\Delta x_{slip}. \quad (6)$$

In equation (6), the first term k_{total} is the total lateral stiffness which can be measured by the slope in Figure 9. The total lateral stiffness is associated with the mechanical strength of the AFM tip and graphene. In addition, Δx_{slip} stands for the lateral displacement due to the slip motion that starts by breaking the AFM tip and graphene adhesion. Thus the nanoscale tip-graphene friction is proportional to two factors: first, the mechanical strength of the tip and graphene; and second, the graphene-tip adhesion strength [80, 87].

Filleter *et al.* [91] reported a twofold increase of friction in monolayer graphene compared to bilayer graphene, which they attributed to the difference in electron-phonon coupling between monolayer and bilayer graphene. Filleter *et al.* [91] used angle-resolved photoemission spectroscopy, and inferred that an efficient energy dissipation mechanism in monolayer graphene originated from efficient electron scattering by the excited phonons.

Using lateral force microscopy, the frictional force between the surface of the graphene and the tip of the Si_3N_4 cantilever was measured by Lee *et al.* [83]. The obtained frictional force ranged from 8.5 pN to 9.5 pN as a function of logarithmic scanning velocity.

When coated on a surface, graphene can cause a significant reduction in frictional forces and in the coefficient of friction [82]. Kim *et al.* [82] found that with a fused silica counterpart in a

microtribometer, the coefficient of friction (COE) is in the range 0.03-0.22 for CVD graphene on different substrates (e.g. Cu- or Ni-grown), which is much less than its COE with SiO_2.

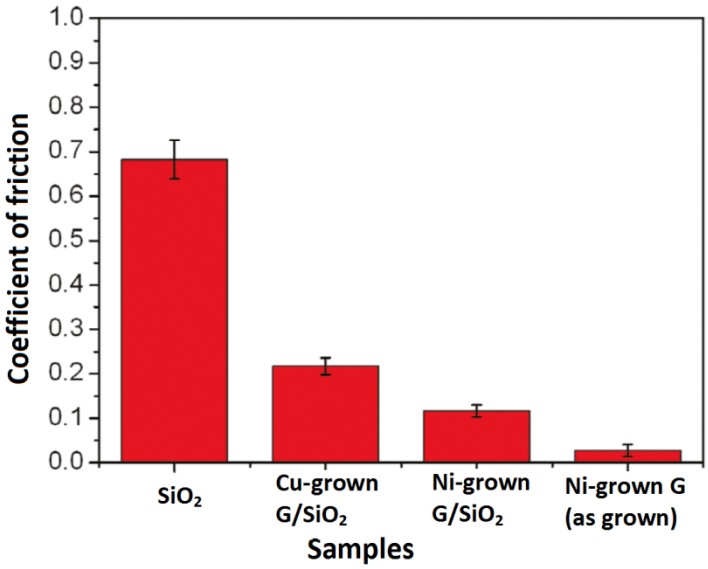

Figure 10. Coefficient of friction for graphene samples (adapted from Ref. [82])

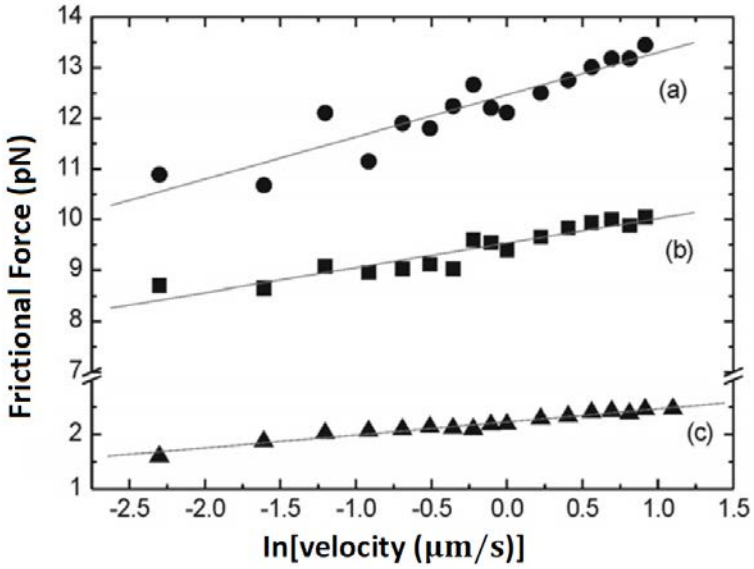

Figure 11. Comparative frictional forces for a) SiO2, b) graphene, and c) graphite (adapted from Ref. [83])

On the other hand, a chemical modification can significantly alter out-of-plane bending stiffness and hence the frictional property of graphene [81]. For example, nanoscale friction is about six times higher for fluorinated CVD graphene than for pristine graphene [80, 81]. Hydrogenated and oxidized graphene have shown doubled and seven-fold increases in friction respectively [80]. The additional dissipation takes place through flexural phonons [81].

An early study into the wear of graphene was done by Li-Yu Lin [95] and his co-workers. With the critical load (5 μN), after 100 cycles of sliding with the Si tip of AFM, a graphene monolayer was removed. At this point, stress generated within the graphene layers exceeds a certain value along the border of the wear track, and the interplanar carbon-carbon bonds break. Thus, failure strength needs to be generated for the initiation of wear in monolayer graphene; and for wear in bilayer or multilayer graphene, higher applied loads are required [95].

3.4. Adhesion

Adhesion is the ability of an interface to resist mechanical separation [96]; in other words, the effective work of fracture per unit area to separate the interface of interest is defined as adhesion. To determine adhesion, an important quantity is the strain energy release rate (G), which is the energy dissipated during fracture per unit of newly created surface area (A) [97] i.e. $G = -\left[\frac{\partial U}{\partial A}\right]$, where U = potential energy available for crack growth. Adhesion is quantified in terms of the critical value of the strain energy release rate G_c (J/m^2). Sufficient interfacial adhesion of graphene with substrate is very important to guarantee structural stability and also the mechanical reliability of the performance for graphene-based microdevice over long periods of time.

Table 3. Comparative study of the adhesion of graphene

Type	**Methodology**	**Interface**	**Adhesion Energy (J/m^2)**	**Author**
Exfoliated or CVD graphene	Blister Test	Monolayer graphene on SiO_2	0.45	Koenig *et al.* [98]
		Two to five layer graphene on SiO_2	0.31	
		Graphene on SiO_2	0.24	Boddeti *et al.* [99]
		Graphene on Cu	0.34	Cao *et al.* [100]
		Graphene on silicon	0.151	Zong *et al.* [101]
	Nano-scratch test	graphene on SiO_x/Si	2.978	Das *el al.* [102]
	Double cantilever beam (DCB) test	Monolayer graphene on Cu	0.72	Yoon *et al.* [103]

Transfer-free graphene	Continuum model and scanning tunneling microscope	3 ± 1 layer graphene on SiC (0001)	$3.0 \pm \frac{1.6}{1.0}$	Wells *et al*. [104]
	Four Point Bending Test	bilayer graphene on SiC (111)	4-8	Iacopi *et al.* [54]

Bilayer or multiple layer graphene sheets having a separation of 0.35 nm are attracted by weak van der Waals forces (figure 12). Likewise, when graphene is transferred to any substrate, the primary force of interaction is the van der Waals force and the adhesion energy is < 1 J/m^2. This low adhesion is not a threat for fabricating a single device in the laboratory. On the other hand, adhesion is several orders of magnitude higher in the case of transfer-free graphene than transferred graphene most likely as a result of the chemical interaction between graphene and the substrate through a buffer layer [104]. For example, interaction between graphene and silicon carbide substrate is mediated by a buffer layer, which is a single layer of carbon atoms [105, 106], and every atom in the buffer layer is covalent bonded to an Si atom underneath; thereby, unprecedented adhesion is achieved [104]. Moreover, the buffer layer could be decoupled from the SiC (0001) by hydrogen intercalation [106] and , whereby adhesion is expected to change.

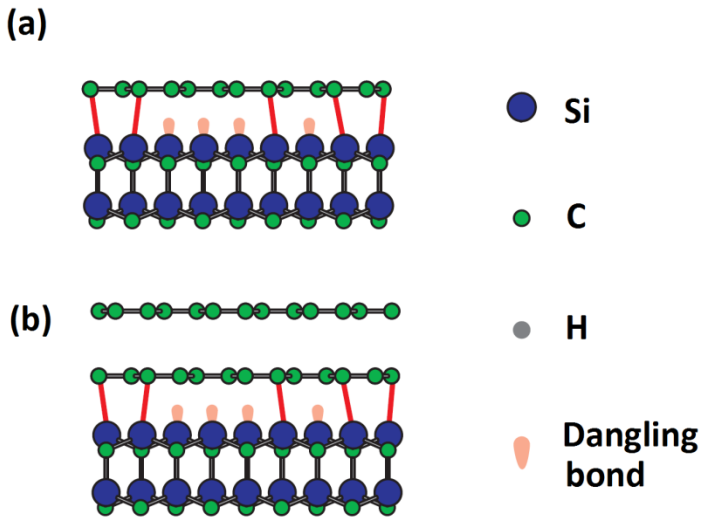

Figure 12. (a) Before and (b) after hydrogen intercalation (adapted from Ref. [106])

High adhesion energies would be extremely useful in graphene straintronics or graphene-based strain sensors, and flexible and stretchable electronics. To influence the graphene bandstructure significantly and to achieve significant electromechanical coupling, a strain as high as 5% or more is necessary. In order to avoid delamination while such a high strain is applied, strong adhesion is needed. Transferred graphene cannot sustain this high strain through the van der

Waals force with the substrate [107]. In order to reach ~5% strain in pressurized graphene blisters, an adhesion energy as high as ~ 3 J/m^2 [108] is required, which is impossible to attain with transferred graphene due to the low reported adhesion energy associated with it.

3.5. Electromechanical Properties

3.5.1. Piezoresistive Property

The piezoresistive effect of graphene is an interplay between its mechanical and electrical properties [109]. The gauge factor (GF) is given by the ratio of relative change in the electrical resistance to the applied mechanical strain [110, 111]. The sensitivity of a strain sensor is described by GF as follows,

$$GF = \frac{R - R_0}{R_0} \Big/ \varepsilon = \left(\frac{\frac{\Delta R}{R_0}}{\varepsilon} \right) = 1 + 2\nu + \left(\frac{\frac{\Delta \rho}{\rho_0}}{\varepsilon} \right) \tag{7}$$

where R_0 and ρ_0 are the resistance and resistivity under zero strain and R is the resistance under strain (ε), ν is the Poisson's ratio, ΔR represents change in resistance and ρ_0 represents change in resistivity.

It is known that the sensitivity of membranes increases as the thickness decreases [19]. Because of the nanometer order of the thickness of graphene, graphene-based piezoresistive sensors demonstrate orders of magnitude higher sensitivity than that of currently available MEMS sensors. The highest reported GF for graphene is 1.8×10^4 whereas for doped polysilicon GF, it is ~30-40 [112]. In addition, the graphene-based pressure sensor outperforms carbon nanotube (CNT)-based pressure sensors as well.

Table 4. Comparative study of piezoresistive properties of graphene

Strain	Gauge Factor*	Description	Purpose	Author
3%	~1.9	Exfoliated graphene	Electronic-Mechanical	Huang *et al.* [61]

			Coupling	
1%	~6.1	CVD graphene on PDMS	Strain sensor	Lee *et al.* [113]
30%	~2	Exfoliated graphene on PDMS	Strain sensor	Wang *et al.* [114]
0.1%	~11.4	Graphene/epoxy composites	Strain sensor	Kim *et al.* [115]
2.5×10^{-4} %	1.8×10^{4}	Si_xN_y/electrode/graphene	AC strain sensor	Hosseinzadegan *et al.* [112]
0.29%	2.92	CVD Graphene on SiO_2	Strain sensor	Smith *et al.* [19]
0.25%	~1.6	CVD graphene on SiN_x	Pressure sensor	Zhu *et al.* [116]
…	~30	Si-based	Pressure sensor	Christel *et al.* [117]
…	~5	Si-based	Pressure sensor	Melvas *et al.* [118]
...	~0.05	CNT-based	Pressure sensor	Fung *et al.* [119]

* For pressure sensors, the unit of the Gauge factor is μV/V/mmHg.

Graphene can act as a membrane through which no standard gases, molecules, or ions can pass, except the hydrogen ion, and it can also withstand a pressure difference larger than 1 atmosphere [120]. Thus, graphene is convenient for making a pressure sensor. For a membrane-based piezoresistive pressure sensor, the sensitivity/gauge factor is given by [116],

$$S = \left(\frac{\frac{\Delta R}{R_0}}{P} \right) = \left(\frac{\frac{\Delta V}{V}}{P} \right) = \frac{\Delta V}{VP}, \tag{8}$$

where R_0 and V are the resistance and voltage respectively when pressure is zero; R is the resistance when pressure difference P is acting on the membrane, and ΔV is the change in voltage.

In general, the key factors that determine the sensitivity ($\frac{\Delta R}{R_0}$) of membrane-based piezoresistive pressure sensors are the thickness and the area. In the case of large deflections relative to membrane thickness, the sensitivity is given by [19],

$$S \propto \frac{\Delta R}{R_0} \propto \sqrt[3]{\frac{P^2 E a^2}{h^2}}, \tag{9}$$

where E is the Young's modulus, a^2 is the area, and h is the thickness of the membrane. Note that in order to avoid noninert gas adsorption and to keep the resistivity independent of the influence of the environment, measurements should be taken in argon gas [19]. Moreover, the sensitivity of the graphene-based pressure sensor can be increased by designing low noise electronics and by optimizing sensing wire patterns [116]. In order to sense high pressure, the adhesion needs to be high enough to prevent the delamination of the graphene from the substrate.

3.5.2. Piezoelectric Property

Assuming the applied electric field vector E and an applied strain tensor σ, the resulting polarized electric displacement vector is D and the produced stress tensor $\in$ are related through converse piezoelectric coefficient c^c and the direct piezoelectric coefficient c^d as follows:

$$\begin{bmatrix} D \\ \varepsilon \end{bmatrix} = \begin{bmatrix} e & c^d \\ c^c & s \end{bmatrix} \begin{bmatrix} E \\ \sigma \end{bmatrix}, \tag{10}$$

where e and s are the dielectric tensor and the elastic compliance tensor, respectively. The direct and converse piezoelectric coefficients are two important parameters that can be used to evaluate the piezoelectric properties of a material. The direct piezoelectric coefficient can be defined as the electric displacement per unit stress at a constant electric field [121]. On the other hand, the converse piezoelectric coefficient can be defined as the strain per unit electric field at constant stress [122]. In 2D materials such as graphene, both of these coefficients are 2x2 tensors.

Intrinsic graphene is 2D in nature, with perfect physical symmetry, and as a result it does not show piezoelectric properties. However, sereral theoretical predictions or experimental demonstrations show that graphene can be modified or engineered to have a piezoreponse. Ong *et al.* [123] used density functional theory and performed a simulation to predict the piezoelectric properties of graphene. By doping one side of the graphene with either Li, K, H and F or doping both sides with different atoms (e.g. H and F; Li and F), they theoretically found significant piezoelectric properties. In another study, Chandratre *et al.* [124] used quantum mechanical calculations to show that porous graphene sheets with holes of the right symmetry can show a piezoelectric coefficient that is nearly 72% of the piezoelectric quartz. In contrast, Wang *et al.* [8] and Rodrigues *et al.* [16] achieved piezoelectric properties of graphene through experimental techniques.

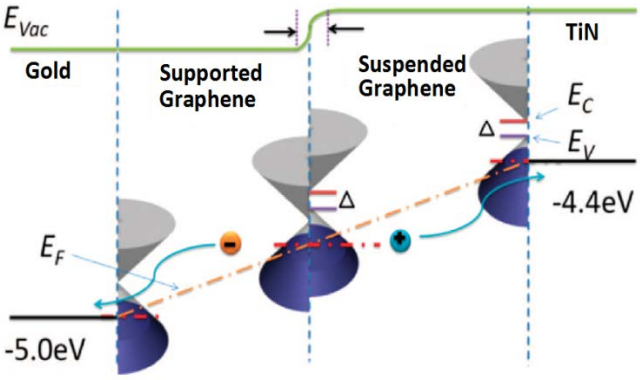

Figure13. Schematic band bending under applied mechanical load (adapted from Ref. [8])

Wang and co-workers [8] applied an in-plane biaxial-strain in a graphene membrane by pressing with an AFM-tip. Across the suspended/supported graphene boundary, biaxial-strain creates band bending. The corresponding work function mismatch separates the charges and accumulates in the space charge region, so polarization is produced. In this recent paper, Wang *et al.* [8] experimentally demonstrated the direct piezoelectric constant as $\sim 37 \mathrm{nCN}^{-1}$ and converse piezoelectric coefficient as $\sim 12.5 \mu \mathrm{m} V^{-1}$.

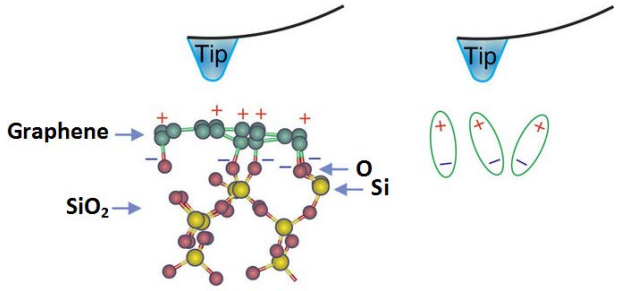

Figure 14. The origin/mechanism of the piezoelectric effect of graphene supported on SiO_2 (adapted from Ref. [16])

Unlike Wang *et al.* [8], who measured the in-plane direct piezoelectric effect of graphene membranes subjected to in-plain biaxial-strain (i.e. under a non-equilibrium condition), Rodrigues *et al.* demonstrated a piezoresponse under a stable equilibrium (static) condition [8]. Rodrigues *et al.* [16] demonstrated that, in the supported graphene on SiO_2, because of the chemical interaction of C atoms with O atoms underneath, a non-zero dipole moment is induced in the vertical direction and results in electrical polarization. Because of the polarization, an in-plane, anisotropic strain as high as $\sim 4-5\%$ was found to be induced on the supported graphene (figure 14). Vertical electric polarization was observed with the help of piezoresponse force microscopy (PFM). The induced high in-plane strain gradient in the supported graphene was

measured by the frequency shift of the G-band of polarization-dependent Raman mapping. There is an excellent correlation between piezoresponse signal distribution and tensile strain distribution. The out-of-plane converse piezoelectric coefficient ($d_{33} = 1.4\ \mathrm{nmV^{-1}}$) found by Rodrigues *et al.* is more than two times higher than the best piezoelectric ceramics of the lead zirconate titanate family [16].

d_{33} = induced strain in z direction per unit electric field applied in z direction

$= 1.4\ \mathrm{nmV^{-1}}$ [16]

4. Nanomechanical Clamped-Clamped Resonator

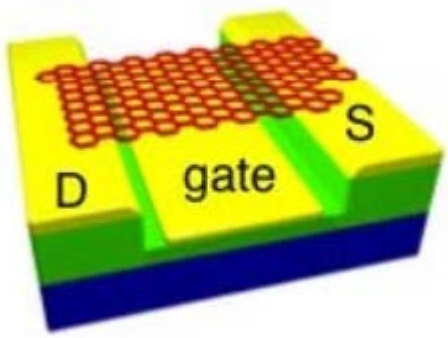

Figure 15. Graphene nanomechanical resonator (adapted from Ref. [125])

A graphene nanomechanical resonator is a monolayer (or few-layers) graphene sheet on a support that oscillates at its natural frequency [20, 126]. Some examples of this are a graphene cantilever [127], a graphene clampled-clamped resonator [128] and a graphene drum resonator [129-132]. A resonator complete with an actuation and readout system can work as a sensor by measuring the shifts from the natural resonator frequencies as the result of an added charge or mass (dynamic response) [133]. The resonator's natural frequency (f_0) reduces as the resonator mass increases, for example due to the adsorption of targeted species on its surface [134].

Another important parameter for dynamic sensing is the quality factor (Q). Q is defined as the stored vibrational energy over the energy loss per cycle of vibration. It can also be defined as

$$Q = f_0/\Delta f\ , \qquad (11)$$

where Δf is the full width half maximum of the response peak [20, 135]. The Q-factor is inversely proportional to damping parameters. It is desirable to increase the resonator's Q as much as possible in order to have minimum mechanical coupling to the surrounding environment and thus minimum energy dissipation to the environment. This further results in high resolution and stability of the resonant sensor [136, 137].

4.1. Electrical Actuation and Detection Schemes

Unlike a silicon nitride or silicon carbide resonator, a graphene-based resonator is electrically conductive and thus is typically actuated and detected by using electrical modulation [138]. The ultrasmall geometric capacitance makes the conventional direct capacitive readout extremely difficult and necessitates frequency mixing methods such as the amplitude modulation (AM) actuation and detection scheme. However, the main drawback of the AM detection scheme is the large noise originated from parasitic capacitance of the gate to the contact pads of the graphene resonator [138]. In order to suppress this noise, the frequency modulation (FM) detection scheme can be used, where a high frequency signal is down converted into a low frequency (~kHz) and therefore the detection is simplified, enabling better detection of the mechanical motion of graphene [140]. Nevertheless the low operating frequency (~kHz) causes significant reduction of the measurement bandwidth making these measurements very time consuming and reduces the speed of detection. Therefore, it has limitations for real-time applications such as mechanical signal processing and radio frequency applications [125][138]. The two frequency mixing methods are discussed in the following subsections.

4.1.1. AM Actuation and Detection Scheme

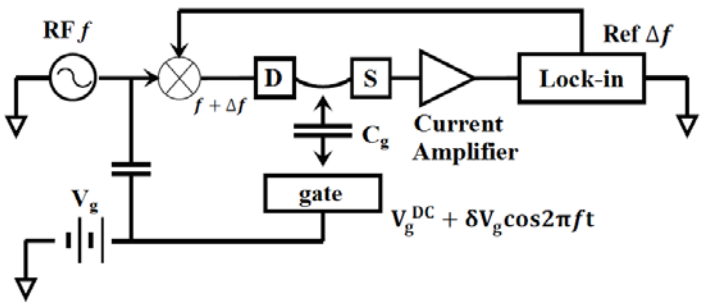

Figure 16. Schematic of a AM actuation-detection scheme (adapted from Ref. [74, 126])

A gate voltage with a DC component (V_g^{DC}) and a small AC component (δV_g) with radio frequency (RF) f is applied to the gate electrode,

$$V_g = V_g^{DC} + \delta V_g \cos 2\pi f t \tag{12}$$

Suppose that the capacitance between the gate and the graphene sheet (placed between the drain (d) and source (S) electrodes) is given by C_g and C_g' , where C_g' is the derivative of C_g with respect to distance between the resonator and the gate. Consequently, an additional charge ($q = C_g V_g$) is induced on the resonator surface, whereas an opposite charge of $-q$ is present on the gate electrode. The attaction between them is given by:

$$F_{el} = \frac{1}{2} C_g' V_g^2 \approx \frac{1}{2} C_g' V_g^{DC} (V_g^{DC} + 2\delta V_g), \tag{13}$$

where F_{el} is the attraction force. The role of V_g^{DC} is to produce a static force on the resonator that enables us to control its tension. On the other hand, the δV_g periodic force sets the resonator into motion. The displacement becomes very large as the driving frequency approaches close to the resonance frequency of the resonator. Thus the resonator is actuated with desired displacement or modulation using the electrostatic force between the resonator and the gate electrode.

A high-frequency mixing approach is used for the readout purposes as shown in figure 16 [74, 126]. For this, an RF signal with frequency of $(f \pm \Delta f)$, $\delta V_{sd}^{f \pm \Delta f}$, is applied to the drain electrode. The magnitude of the current ($I^{\Delta f}$) is measured by a lock-in amplifier and then δz^f which is the amplitude of vibration at the driving frequency (z is the graphene-gate distance), is calculated using the following equation (14) [139].

$$I^{\Delta f} = \delta G \delta V_{sd}^{f \pm \Delta f} = \frac{dG}{dV_g} \left(\delta V_g + V_g \frac{\delta z^f}{z} \right) \delta V_{sd}^{f \pm \Delta f}, \tag{14}$$

where δG is the modulated conductance. The first term in parentheses, δV_g, is nonzero at any driving frequency and only shifts the current curve. In contrast, the second term δz^f, is obtained from the resonator vibration. Consequently, the δz^f value changes significantly as the driving frequency approaches the resonance frequency. The Q can be obtained afterwards using the respective frequency and associated δz^f.

4.1.2. FM Actuation and Detection Scheme

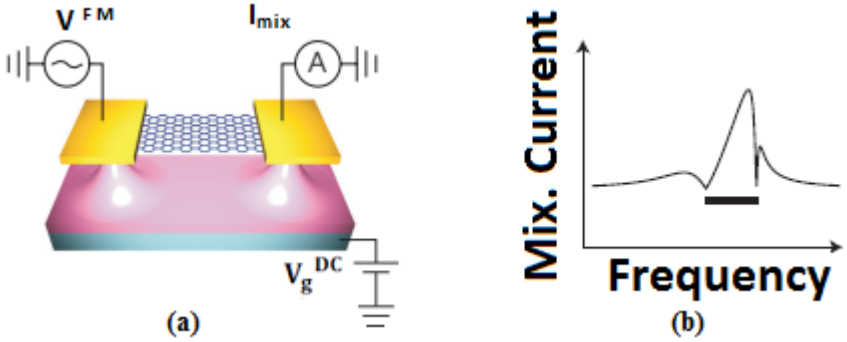

Figure 17. a) Schematic of the FM actuation/detection scheme, b) Frequency response showing nonlinear damping of the mixing current (adapted from Ref. [21])

The FM detection scheme (figure 17), which is simpler and yet more noise tolerant as compared to AM detection scheme, was first applied to carbon nanotubes resonators [140] and later to graphene resonators [21, 135] to detect the mechanical motion.

In the FM detection scheme, a frequency-modulated voltage, V^{FM}, is applied to the source electrode of the resonator. In this case, a low frequency (f_L) signal from the lock-in amplifier is sent to FM input of an RF generator. Consequently, the RF generator outputs a frequency-modulated voltage, V^{FM}.

$$V^{FM} = V_{AC}\cos(\Psi(t)), \tag{15}$$

$$\text{where, } \Psi(t) = \left[2\pi ft + \left(\frac{f_\Delta}{f_L}\right)\sin(2\pi f_L t)\right]. \tag{16}$$

and V_{AC} is the amplitude (alternative current voltage) of the frequency-modulated voltage. In equation (16), f is the carrier frequency and $f_\Delta$is the frequency deviation between the low frequency and the carrier frequency.

As a result of this frequency-modulated voltage, the resonator starts vibrating and the motion (the real part of its oscillation amplitude: $Re[x_0]$) is calculated from the measured mixing current at f_L following equation (17). The current measurement is performed through a lock-in amplifier [138, 140].

$$I_{mix} = \frac{1}{2}\frac{dG}{dV_g^{DC}}.V_g^{DC}.\frac{C'}{C}V_{AC}.f_\Delta\frac{\partial}{\partial f}\mathrm{Re}[x_0], \tag{17}$$

where V_g^{DC} is the gate voltage, C is the gate-resonator capacitance and $C'$is the first derivative of the C. The Q can be calculated afterwards following figure 17 (b) and equation (17).

4.2. Dynamic Resonant Sensing Parameters

4.2.1. Resonance Frequency

Assuming zero bending stiffness of graphene, the resonant frequency of fundamental mode of a graphene clamped-clamped resonator is given by [126, 136],

$$f_0 = \frac{1}{2L}\sqrt{\frac{T + T_e(V_g)}{\rho h}}, \tag{18}$$

where L stands for the length, h represents the thickness, T stands for tension in the resonator, $T_e(V_g)$ = external tension induced by electrostatic force, and ρ is the material density. Chen *et al.* [126] experimentally demonstrated that the resonant frequency scales inversely with the length of the graphene resonator. When $T_e(V_g) = 0$, then [136]

$$f_0 = \frac{1}{2L}\sqrt{\frac{T}{\rho h}} = \frac{1}{2L}\sqrt{\frac{\sigma}{\rho}}, \tag{19}$$

where σ represents the tensile stress in the resonator.

It is evident from equation (19) that the resonant frequency of clamped-clamped resonators increases upon application of tensile stress. One way to increase the tensile stress is through the application of DC gate voltage at room tempretaure, where the resonator tensile stress increases as the voltage increases. Another way to increase the tensile stress is through thermal effects [74, 126]. This has been shown for both below and above room temperatures. The first case applies for a graphene resonator with metal electrodes. In this case, the graphene resonator needs to be cooled down to a temperature below 300 K to have a negative CTE. This further results in the expansion of the graphene resonator and the contraction of the metal electrodes and thus the increase of tensile stress within the graphene resonator. The second case is applied to a graphene resonator with SU-8 anchors with annealing temperatures between 673 K to 873 K as shown in figure 18. Here, the SU-8 resist anchors contract and the graphene resonator expands as the result of annealing. Annealing temperatures above 873 K resulted in the fracturing of the graphene resonator anchors. A maximum of 1 GPa tensile stress was measured at 873 K annealing temperature [136]. SU-8 clamped graphene drum resonators demonstrated similar

behaviour where hard baking of SU-8 resulted in increased strain and an order of magnitude higher resonant frequency [141]. A recent paper of Chen *et al.* [142] demonstrated that, other than tensile stress, chemical potential variation can also result in the resonant frequency shift of a graphene resonator.

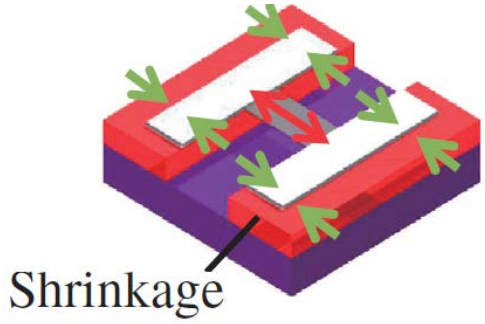

Figure 18. Strained graphene resonator (adapted from Ref. [136])

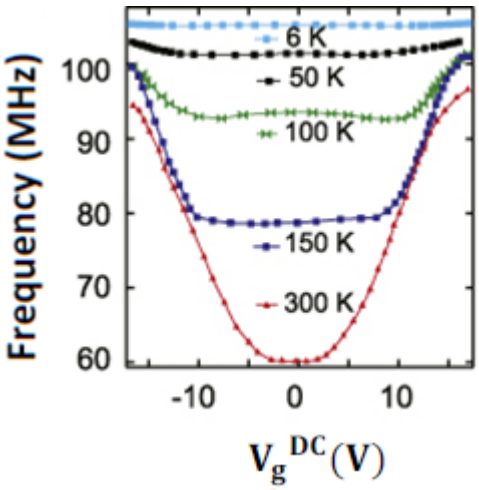

Figure 19. Dispersion of an electromechanical mode in graphene resonator as a function of temperature (adapted from Ref. [74])

Resonator frequency tuning is a critical parameter for various applications. Figure 19 shows DC gate voltage vs. frequency for clamped-clamped graphene resonators as temperature reduces from room tempreture (300 K) to 6 K. It can be seen that frequency tunability reduces as the temperature reduces. So at low temperatures, even though the frequency is high, the frequency tuning is minimal. This limits the application range of the graphene clamped-clamped resonator and thus is not desirable. Drum resonators also demonstrates similar characteristics. Chen *et al.* [143] fabricated micrometre-size graphene drum oscillators whose frequencies can be electrostatically tuned by as much as 14% at room temperature.

The major drawback of graphene nanomechanical resonators is the low reported quality factor at room temperature [20, 126, 144, 145], which is evident from Table 5. This table shows various reported values of resonant frequency and quality factor for graphene resonators.

4.2.2. Quality Factor

At room temperature, the *Q* factor of graphene nanomechanical resonators is significantly lower than that of the Si_3N_4 resonator. Molecular dynamics (MD) simulations [146, 147] attributed the low *Q*-factor of these mono to few atomic layers graphene nanomechanical clamped-clamped resonators at room temperature to the flipping of the free edges of the clamped-clamped resonator which destroy the coherence of the mechanical oscillation [135].

To overcome the low *Q* of the room temperature operation of graphene nanomechanical clamped-clamped resonators, lower temperatures can be used. It has been shown that at low temperatures, graphene NEMS clamped-clamped resonator *Q* is affected by the nonlinear dissipation term of the equation of motion unlike the room temperature where the linear dissipation term is dominant [21, 148]. Thus, graphene NEMS clamped-clamped resonator *Q* is highly temperature dependant unlike thicker NEMS resonators fabricated from the Si_3N_4 resonator or stressed SiC resonator on Si [149].

The *Q* of graphene NEMS clamped-clamped resonators at low temperature where nonlinear dissipation is dominant can be approximated from;

$$Q = \frac{1.09\, f_0}{\Delta f}. \tag{20}$$

The temperature (*T*) dependency is further devided to two temperature regions as shown in equation (21) and (22). For a temperature region from 100 to 300 K, the energy dissipation (Q^{-1}) is proportional to square of temperature [150]. Whereas for temperatures below 100 K, the Q^{-1} changes with slower trend and roughly with $T^{0.3-0.4}$ [126].

$$\frac{1}{Q} \propto \mathrm{T}^2 \text{ for } 100\mathrm{K} \leq T < 300\mathrm{K} \tag{21}$$

$$\frac{1}{Q} \propto \mathrm{T}^{0.3\text{-}0.4} \text{ for } T < 100\mathrm{K} \tag{22}$$

$Q \sim 10^5$ [21] has been reported for graphene clamped-clamped resonators at mK range temperature, which is closer to that of a highly stressed Si_3N_4 or epitaxial silicon carbide resonators at room temperature ($Q \sim 10^6$ [149]).

Despite of showing relatively low quality factor at room temperature, the graphene resonator is still promising because of its high Young's modulus and large surface-to-volume ratio.

Table 5. Mechanical f_0 and Q for clamped-clamped graphene resonators with different number of layers and length-width geometries and at different temperatures, actuated electrically. The measurements were all performed at high vacuum (pressure < 10^{-5}). Mass resolution can get as low as 2zg.

Substrate	Layer No.	Length (μm)	Width (nm)	Q	f_o (MHz)	T (K)	Author
SiO_2/Si	few-layer	5	~1930	20-850	1-170	300	Bunch *et al.* [20]
SU-8 resist/SiO_2	5	10	~300	7723	15.91	293	Oshidari *et al.*[136]
Si/SiO_2	…	…	…	10^4	~34	77	Xu *et al.* [125]
Si/SiO2	1	0.5-2	200-2000	1.4×10^4	~130	5	Chen *et al.* [126]
SiO_2	1	2	800	10^5	~156.1	0.09	Eichler *et al.* [21]

To overcome the problem of the flipping of the free edges of the graphene clamped-clamped resonators, drum resonators can be used. Unlike the clamped-clamped graphene resonator, the drum resonator has all sides clamped to the substrate, the edge vibrational modes are absent and the energy dissipation is less. Therefore, the drum resonator shows comparatively higher Q-factor (e.g. $Q \sim 2400$ at room temperature [129]). The primary dissipation mechanism is believed to be phonon scattering which is very intrinsic in nature and as a result, Q is inversely proportional to the temperature (T) [138, 148],

$$\frac{1}{Q} \propto \text{Temparature for } 20\text{K} < T < 300\text{K} \tag{23}$$

It has been reported that the Q increases as the drum diameter [129, 130, 151] and tensile stress [134] increases. Robinson *et al.* [152] fabricated reduced grapheneoxide (r-GO) drum resonators by solution-based transfer process. Because of built-in tension, Q-factors (1500 to 4000) and

frequency (14-54 MHz) exceeded those of pure graphene resonators at room temperature of similar geometries. In addition, high quality factor (Q =31000) at room temperature was reported using chemically modified multilayer graphene (CMG) film [153].

5. Potential of Graphene in MEMS

Although silicon has dominated MEMS technology for the last two decades, it is anticipated that graphene will outperform this in the near future. The unique combination of outstanding mechanical, thermal, electromechanical and electrical properties of graphene is integral to the ever-increasing potential for graphene-based devices. The remarkably higher thermal conductivity and high current-carrying capacity of graphene allows its use as interconnects in graphene-based chips, potentially replacing copper. A graphene based touch panel has superior optical transmission, less sheet resistance and it can withstand more strain than currently available MEMS touch panels e.g. the ITO touch panel [9]. Exfoliated graphene could be used in fuel cells, batteries, inks, conductive coatings, and polymer composites.

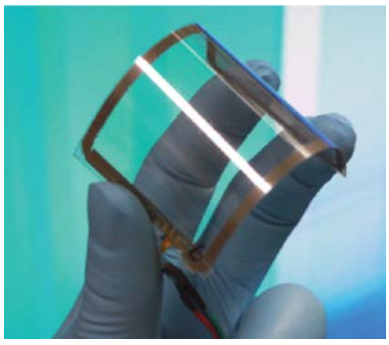

Figure 20. Flexible graphene/PET touch panel (adapted from Ref. [9])

5.1. Graphene Resonator

The ultimate limit of two-dimensional nanoscale resonators are graphene resonators [20], because they are only one atom thick, and even a few deposited atoms make up a significant fraction of the mass of graphene itself. Graphene has a higher Young's modulus, larger surface-to-volume ratio than a current MEMS resonator. Therefore, fabrication of high frequency and high Q resonators from graphene would be possible in future. Graphene-based resonators could be used as charge sensors [20], precision measurements of mass [126, 154], and as weak or

ultralow force measurements [21]. Whereas single-molecule mass detections are possible with NEMS resonant sensors [19], graphene-based resonators have the potential for detecting a single atomic mass [74, 109]. Unlike state-of-the-art Si_3N_4 and SiC resonators, graphene resonators are good conductors; so an integrated readout from a graphene nanomechanical resonator could be performed easily with good signal-to-noise ratio [126]. Futher applications of graphene nanomechanical resonators are as MEMS voltage controlled oscillators (VCOs) [143] and in quantum information technology [155, 156]. MEMS voltage controlled oscillators (VCOs) have large footprints and also the frequency tuning is difficult at high operating frequency. Graphene VCO, consists of graphene nanomechanical resonators, demonstrates smaller footprints, large frequency tunability at room temparature and therefore, can be efficiently used in transmitting the audio signal [143]. Moreover, graphene resonators are promising in quantum information technology because it demonstrates dynamical intermodal coupling [156].

5.2. Pressure and Strain Sensor

In MEMS, the application of the piezoresistivity of graphene is found as a pressure sensor [17, 19, 116], strain sensor [18, 115, 157], and potentially acceleration sensor [158]. Graphene-based strain/pressure sensors have higher sensitivity yet are smaller in dimension than conventional Si-based sensors. Silicon-based piezoresistive sensors have typical length in the order of hundreds of microns, whereas a graphene-based sensor would result in just a few microns in length [19, 159]. Because of their smaller area and lesser thickness, normalized sensitivity is orders of magnitude higher for graphene-based pressure sensors than that for conventional Si-based piezoresitive pressure sensors [116]. Its transparency, flexibility and piezoresistive properties pave the way for using the graphene-based strain sensor as a touch screen. In addition, flexible graphene-based strain sensors have potential biological applications e.g. in making artificial electronic skin [160], and for finger movement detection [157]. Graphene could be engineered to respond to strain as high as 100% [157], which is useful because human joint movement generates up to 55% strain upon stretching and contracting [161].

5.3. Piezoelectric Actuator and Energy Harvester

Until June 2015, the missing aspect of graphene MEMS was piezoelectric transduction. Wang *et al* [8] and Rodrigues *et al* [16] demonstrated that although unstrained pristine graphene does not show piezoelectric properties at all, applying strain or engineering graphene can lead to piezoelectric properties which are comparable to, or better than, those of conventional

piezoelectric materials. Recently engineered piezoelectric properties of graphene have paved the way for future applications such as in motors, actuators, sensors, energy harvesters, resonators and so on.

5.4. Flexible Sound Source and Ultrasonic Sound Production

As opposed to normal commercial earphones, graphene-based thermoacoustic earphones have demonstrated a capablility of delivering sound of up to 50 kHz; and numerical simulation has predicted that sound frequency of up to 1 MHz is achieveable [162]. Thus the frequency response of graphene-based thermoacoustic sound sources is in the audible range of different animal species, and so has the potential to be suitable for inter-communication between humans and other animals [162]. Moreover, because of its mechanical robustness, atomic thickness, and transparency, single-layer graphene exhibit the potential for flexible, stretchable and transparent loudspeakers [163].

6. Examples of Applications

6.1. Graphene-based Sound Generator

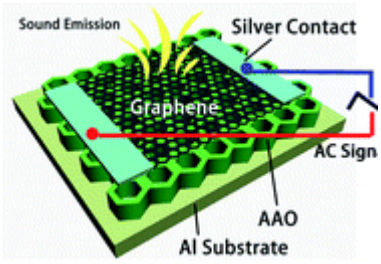

Figure 21. Schematic of thermoacoustic sound generator (adapted from Ref. [164])

Graphene-based thermoacoustic generators are capable of generating sound beyond the audible range [165]. Low heat capacity per unit area (HCPUA) and minimum heat loss to the substrate are two essential pre-conditions for an efficient thermoacoustic sound emission [163]. These conditions can be met through using monolayer graphene because of its minimal thickness (0.335 nm) [164]. The combination of exceptional mechanical and thermal properties suggests that graphene is a suitable material for fabricating thermophones [163, 166]. Tian *et al.* [165] first demonstrated that graphene-based thermophones are capable of producing audible and

ultrasound sound frequency through thermoacoustic effect. When an alternating current is applied to graphene, a temperature oscillation takes place which results in density and pressure oscillation in air; thus, sound waves are produced [165]. Monolayer graphene films on PET or PDMS could also function as transparent and flexible thermophones [162, 163, 167]. On the other hand, in order to minimize heat leakage, Fei *et al.* [166] employed 3D graphene foams (GFs) produced on nickel by CVD and therefore, operating voltage significantly drops to 3V. Heat leakage could also be minimized by using porous substrates such as porous anodic aluminum oxide [164].

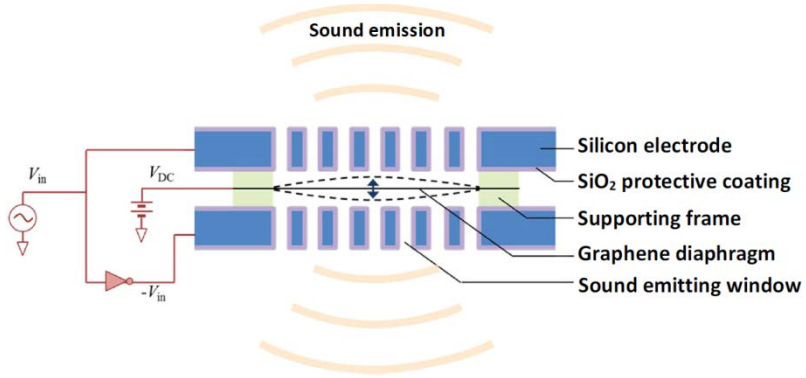

Figure 22. Schematics of the electrostatically driven graphene-based speaker (adapted from Ref. [168]

In general, the major limitation of thermoacoustic graphene generators is their low power efficiency. Hence, for a more efficient generation of sound in the audible range, Zhou *et al.* [168] fabricated an electrically driven graphene-based audio speaker, in which the diaphragm vibrates mechanically and which has comparable or better efficiency than existing commercial counterparts. This audio speaker has a power efficiency six times higher than that of thermophones [168].

6.2. Graphene Coating and Lubrication

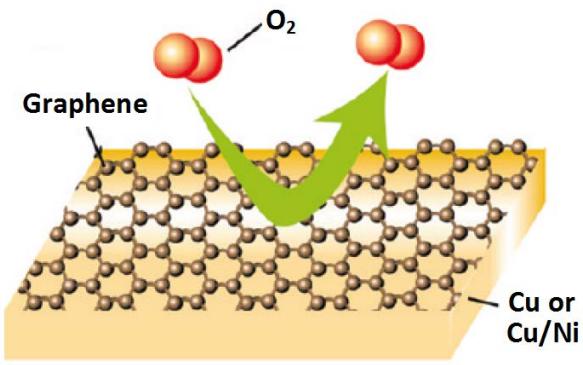

Figure 23. Schematic illustrating single layer graphene as an oxidation barrier (adapted from Ref. [40])

Graphene can function as a protective coating for nanoelectronic devices [169]. Graphene can form the thinnest transparent protective layer on different materials of interest because monolayer graphene has a 0.34 nm thickness [170] with 97.7% ideal transmittance [171]. Moreover, both under room temperature and at elevated temperatures, graphene shows chemical inertness, exceptional thermal stability, and impermeability to gas diffusion [40]. All these properties enable a graphene layer to better protect metals from surface oxidation than any other material [37, 169]. For instance, Chen *et al.* demonstrated that graphene films grown by CVD can protect the surface of Cu and Cu/Ni alloys from air oxidation even after heating at 200°C in air for up to 4 hours [40]. On the other hand, CVD graphene can protect Ni substrate surfaces from oxidation even after heating at 500°C in air for up to 3 hours [169]. The corrosion occurs through the defects [37, 172] or coating discontinuities or lifting [173] of graphene. A corrosion inhibiting coating (in which pre-annealed (at 600°C) Cu-foil was coated with acetone and annealed at 1000°C), , with fewer defects than CVD, has been reported by Huh *et al.* [174]. Graphene could replace conventional coating layers and act as a better metal protection layer provided that it is without defects and grain boundaries, from where corrosion originates [40, 175]. Graphene corrosion protection coating would work on Cu, Fe, Ta, Pt, Ir, Ru [40, 169]. The efficiency of the corrosion protection coating would be significantly enhanced by producing large-grain graphene with high uniformity and ensuring high fidelity of mechanical transfer [37]. In addition to corrosion protection coating, different types of hybrid coating for devices could be prepared using graphene such as self-cleaning or anti-fouling coating [176-178] and fire retardant coating [179-181].

Due to its exceptionally low friction behavior, graphene coating is an excellent choice for solid lubrication and for wear- and scratch-resistant coatings. A few layers of graphene can be used as

a solid lubricant for tribo-pairs consisting of stainless steel surfaces open to the air and the coefficient of friction (COF) is 6 times lower if graphene is used [182]. Graphene forms a conformal protective coating on the sliding contact interfaces, facilitating shear, and slows down the tribo-corrosion, thus reducing wear by 4 orders of magnitude [182] until graphene transforms to amorphous carbon [183]. Moreover, in contrast to graphite-based lubricants which work well only in humid conditions, graphene shows reduction in the coefficient of friction and wear under dry and inert test conditions as well [184]. Graphene could be used as a lubricant on SiC-based MEMS and NEMS [90], and on different substrates like silicon oxide [83, 84], and copper foils [185].

In a recent study, Berman *et al.* [186] reported that graphene coated nanodiamonds can show macroscopic superlubricity against diamondlike carbon (DLC), and the resulting COF is as low as ~0.004 in a dry environment. Nanoscrolls are formed when graphene patches are wrapped around nanodiamonds; thus the contact area with the DLC is significantly reduced, and this leads to superlubricity.

6.3. Piezoresistive Sensors

In a piezoresistive sensor, a change in resistivity allows us a read-out of strain or pressure. Several types of graphene-based materials, e.g. suspended graphene over a cavity [19], a nanographene island [18], a stretchable graphene nanopaper made of cellulose and graphene [157], a graphene/epoxy composite [115], and a film stack membrane [112], use the piezoresistive effect to make strain sensors and pressure sensors. Note that the graphene drumhead can confine $\sim(\mu\text{m})^3$ of gas, and would potentially act as an ultra-small pressure sensor [120].

6.3.1. Pressure Sensors

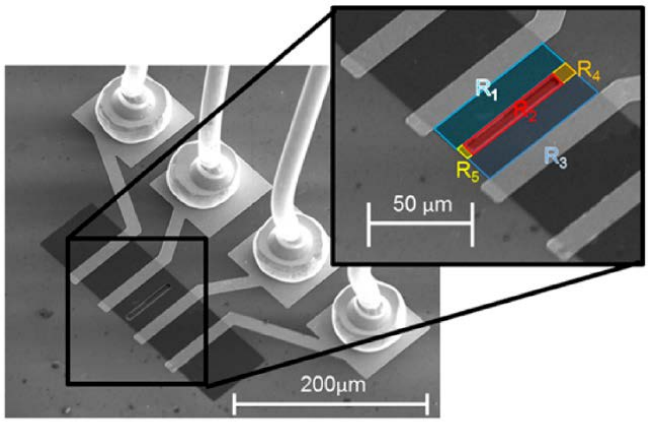

Figure 24. Different resistor components for calculating the gauge factor of a pressure sensor (adapted from Ref. [19])

Smith *et al.* [17, 19] fabricated a pressure sensor by suspending CVD graphene on a 1.5 μm deep rectangular cavity etched by RIE. To create contacts, another four RIE etched cavities were first filled with titanium and next with gold, using metal evaporation. Then the graphene was transferred over the cavity and finally, the strain gauge was wire bonded. In order to measure GF, Smith *et al.* [17] placed a graphene membrane as a resistor (R_2) in a wheatstone bridge. Because of the piezoresistive effect, the initial resistance (R_2) of the graphene just above the cavity, changed with the change of pressure, whereas resistances from other parts (R_1, R_3, R_4, R_5) were constant. The ratio of the change in resistance to the change in strain gives the GF of the pressure sensor as 3.67 [19].

Zhu *et al.* [116] fabricated a pressure-sensing device utilizing the piezoresistive effect of multilayer CVD graphene on top of a square silicon nitride membrane, and their reported gauge factor was ~1.6 for the differential pressure range from 0 to 700 mbar.

6.3.2. Strain Sensors

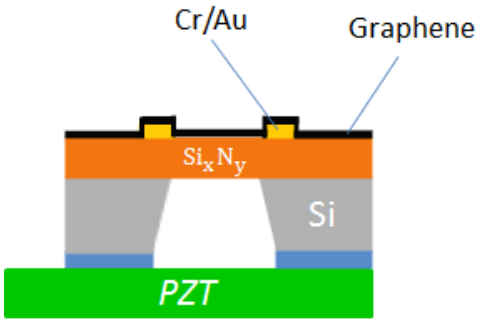

Figure 25. A graphene-based MEMS strain sensor (redrawn from Ref. [112])

Hosseinzadegan *et al.* [112] made a film stack comprised of a low stress-Si_xN_y, Cr/Au electrode and graphene. For actuation purposes, a PZT actuator was used to excite the first breathing mode of the film stack. In order to estimate the change in the resistance of the film stack membrane, the voltage between the inner Cr/Au electrodes of a four-point probe was measured. The displacements obtained from the optical interferometer in conjunction with finite element simulations, gave an estimation of strain at each point. In the plot of change in resistance vs. AC strain, the slope represents the gauge-factor ($\sim 1.8\times10^4$) for a few-layer graphene membrane [112].

Zhao *et al.* [18] explored nanographene for sensing strain through piezo-resistivity. Quasi-continuous nanographene (NG) films were directly deposited on fluor-phlogopite mica substrates by PECVD with tunable sizes, densities, and layers. Under strain, a significant variation in resistance arises from the change of charge tunneling between neighboring NG islands, giving rise to large piezoresistive GF ($\approx$ 300). The main advantage of the high sensitivity NG-based strain sensor is that the gauge factor can be tuned by controlling the initial sheet resistances of NG films.

Kim *et al.* [115] took another approach to make a strain sensor from a hybrid material made of graphene and epoxy. In this hybrid material, the contact area of the adjacent nanofiller was reduced upon tension and the contact resistance was increased, which lead to the higher resistivity of the strain sensor composites. This strain sensor showed symmetrical and reversible strain with reported GF $\approx$ 11.4 within 0.1% strain.

In order to make a strain sensor, Yan *et al.* [157] mixed crumpled graphene with nano cellulose, filtering it in a vacuum and made 'flexible nanopaper'. Then 'stretchable nanopaper' was obtained by embedding the 'flexible nanopaper' in polydi methylsiloxane (PDMS). The 'stretchable graphene nanopaper' can be stretched up to 100% with 1 mm thick substrates and is capable of sensing in all directions, due to the soft nature of PDMS.

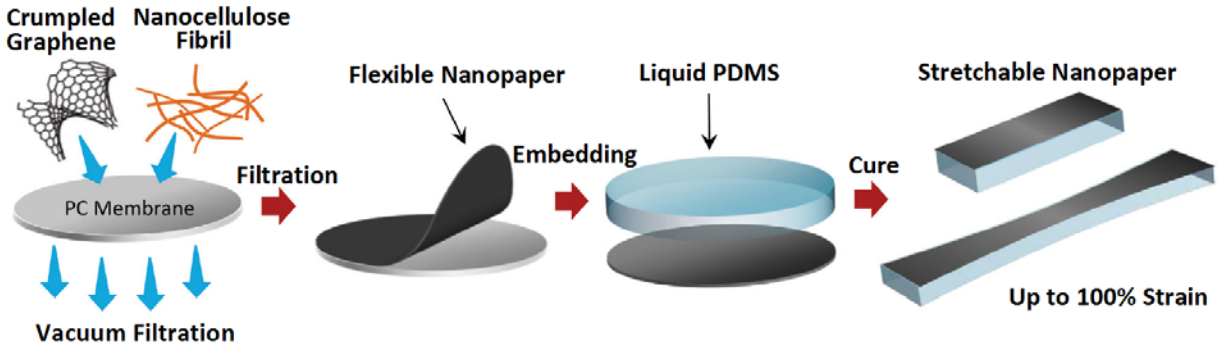

Figure 26. Fabrication processes for stretchable graphene nanopapers (adapted from Ref. [157])

6.4. Resonant Sensors

A graphene resonator with a uniform gap was fabricated by transferring graphene to the substrate and then etching the underlying oxide using buffered hydrofluoric acid (BHF) [21, 126]. In order to avoid breaking the suspended graphene because of surface tension, transfer to another solution (i.e. water, acetone, ethanol etc.) and critical point drying [187] were used.

Another way of fabricating a graphene resonator is using predefined trenches on SiO_2 substrates and transferring exfoliated/CVD grown graphene sheets to that substrate [20, 144]. Bunch *et al.* [20] made these predefined trenches by etching an SiO_2 surface with dry RF plasma. In all cases, the electrodes are defined by e-beam photolithography.

6.4.1. Mass Sensing

Unlike conventional resonators, graphene has a two-dimensional structure, large exposed surface area and large surface-to-volume ratio, which make the interaction with external masses convenient [151]. Moreover, graphene resonators have high operating frequencies which make it very efficient for sensing applications [20] [21]. Thus for atom or molecular mass sensing, or atomic dust-detecting [188], a graphene mechanical resonator is promising.

In general, the technique that a graphene-based mass sensor utilizes is the correlation between the mass of the attached object and the resonator's resonant frequency. Several studies [188-190] have demonstrated that mass added to the resonator results in a decrease in a mass sensor's resonance frequency.

If M_{eff} is the effective vibratory resonator mass of the resonant mass sensor, f_0 represents the resonant frequency of the sensor without external mass and the minimum detectable frequency shift is δf_0, then the minimum detectable mass (also known as mass resolution) of the system is given by [138, 189, 191-193],

$$\delta M \approx \frac{\partial M_{eff}}{\partial f_0}\delta f_0 = R^{-1}\delta f_0 = -2\frac{M_{eff}}{f_0}\delta f_0 . \tag{24}$$

where $R = \frac{\partial f_0}{\partial M_{eff}} = -\frac{f_0}{2M_{eff}}$ is the mass responsivity of the mass sensor.

Therefore, responsivity can be increased by increasing f_0 and reducing the dimensions of the resonator to make the mass lower. For a supported rectangular graphene resonator, Lee *el al.* [188] reported the theoretical value of the inverse of responsivity (R^{-1}) of 10^{-27} g Hz^{-1}, whereas the experimental value of (R^{-1}) reported by Chen *et al.* was $2x10^{-15}$ g Hz^{-1} [126] for a clamped-clamped graphene resonator. Wong *et al.* [130] reported that a mass sensor made of circular graphene membrane has a theoretical R^{-1} of 10^{-20} g Hz^{-1}. On the other hand, the reported inverse mass responsivity of silicon-based resonators ranges from 10^{-12} g Hz^{-1} to 10^{-18} g Hz^{-1} [130, 189, 190].

The minimum detectable frequency shift is δf_0 against a background of noise is [194],

$$\delta f_0 = \frac{f_0}{Q}.10^{-DR/20} . \tag{25}$$

where *DR*=dynamic range.

Therefore, from equation (24), we obtain the minimum detectable mass as [126],

$$\delta M = -\frac{2M_{eff}}{Q}.10^{-DR/20}, \tag{26}$$

If the current noise spectral density of the measurement is represented by $S_n^{1/2}$, then the mass sensitivity, $S_m^{1/2}$ is given by [126],

$$S_m^{1/2} = \frac{\partial M_{eff}}{\partial f_0}\frac{\partial f}{\partial I}S_n^{1/2}, \tag{27}$$

where, $\frac{\partial f}{\partial I}$ is the slope of the response function.Chen *et. al.* [126] estimated the mass sensitivity as 7.6x10-15 $g/\sqrt{Hz}$ for the fabricated graphene resonator.

Two other important factors for mass sensing are the control over resonant frequency and its tunability. Singh *et al.* [74] reported that the built-in tension, the added mass and the thermal expansion of graphene determine the resonance frequency and the tunability of a graphene mass sensor. They also found that the tunability of the resonant frequency is sufficient at room temperature for mass sensing purposes, but it is poor at low temperature [74].

6.4.2. Force and Charge Sensing

The ultimate limit on force sensitivity is given by [20],

$$dF^f = \left[\frac{4\kappa_{eff}(k_B T)}{f_0 Q}\right]^{1/2}, \quad (25)$$

with the effective spring constant, $K_{eff} = m_{eff} f_0^2 = 0.735 Lwt f_0^2$ where L, w and t are the length, the width and the thickness of the resonator, respectively.

Force sensitivity is inversely proportional to the square root of resonant frequency, f_0 and the Q-factor. So, force sensitivity is very high when f_0 and Q are very high, but the temperature is very low. An increase in force sensitivity is limited by thermal oscillation in the resonator, even when it is not being driven. The root mean square (RMS) amplitude of thermal oscillation is given by $x_{th} = \left[\frac{K_B T}{K_{eff}}\right]^{1/2}$. Bunch *et al.* [20] calculated the force sensitivity to be 0.9 fN/ $Hz^{1/2}$ for a resonator with dimensions t = 5 nm, L = 2.7 mm, and w = 630 nm, and having a resonance frequency f_0 = 35.8 MHz and Q = 100 at room temperature. Note that in this case, thermal RMS motion is x_{th} = 76 pm.

For a distance '*d*' between the graphene sheet and the gate electrode, the charge sensitivity is given by,

$$dQ^f = dF^f \left(\frac{d}{V_g^{dc}}\right) = \left(\frac{d}{V_g^{dc}}\right)\left[\frac{4\kappa_{eff}(k_B T)}{f_0 Q}\right]^{1/2}. \quad (26)$$

Bunch *et al.* [20] calculated that the charge sensitivity is $8x10^{-4}$ e/ $Hz^{1/2}$ at room temperature. However, as lowering temperatures will result in higher quality factors and thus higher charge sensitivity, the graphene resonator would be a potential competitor of RF single-electron transistor electrometers, having a charge sensitivity of $1x10^{-5}$ e/ $Hz^{1/2}$ [20].

6.5. Piezoelectric Transduction

6.5.1. Nanogenerator

Wang *et al.* [8] designed a nanogenerator from the two-dimensional piezoelectric effect of a suspended graphene membrane. They fabricated the holes ($\sim 3\mu$m) on the substrate using photolithography and reactive ion etching and, after that, graphene was deposited by mechanical cleavage and exfoliation. Finally, to fabricate electrodes on the graphene, they used the lithography-free process, a good way to avoid breaking the suspended graphene membrane (figure 27a) [8]. The open circuit voltage was minimized by choosing gold as the cathode and an AFM tip as the anode, which have high and low work functions respectively. The band bending from the AFM-tip-generated-deformation resulted in a forward output voltage because the separated charges can accumulate on external electrodes. The nanogenerator's output current characteristics can be obtained by replacing a voltmeter with an ammeter (figure 27b).

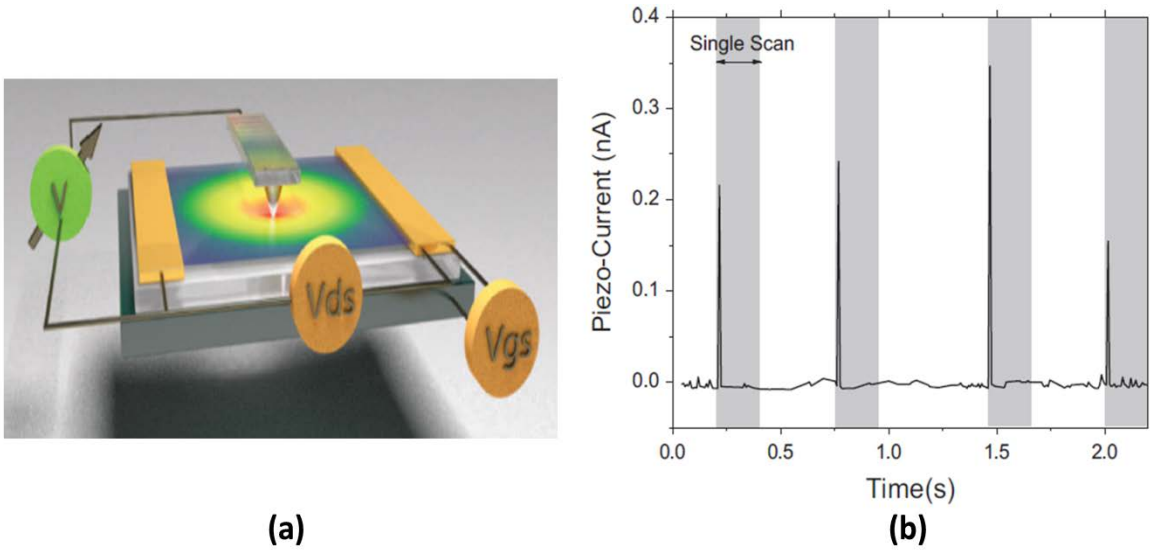

Figure 27. (a) Schematic of nanogenerator containing a monolayer graphene channel; b) Short circuit current of the nanogenerator made of graphene membrane (adapted from Ref. [8])

6.5.2. Actuator

A recent experimental demonstration of piezoelectric properties was given by Rodrigues and co-workers [16]. They used a SiO_2 calibration grating that had a series of parallel rectangular grooves of 1,317±10 nm height, with a periodicity of 1,500±10 nm, as a substrate (figure 28). They transferred monolayer graphene (produced by CVD) onto this SiO_2 grating substrate,

which has oxygen termination. Thus a series of supported and unsupported graphene layers was formed on the SiO_2 grating substrate where the supported parts gave rise to piezoectric properties. With the reported piezoelectric constant $d_{33} \approx 1.4\,\mathrm{nmV^{-1}}$, Rodrigues *et al.* [16] have predicted the graphene/SiO_2 structures as a potential platform for fabricating nano-actuators.

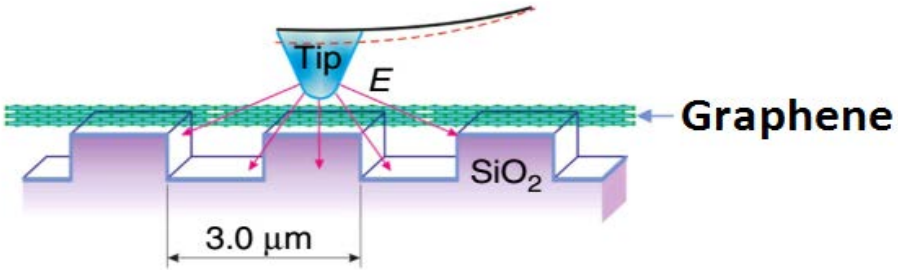

Figure 28. Schematic of graphene-SiO_2 nanoactuation platform (adapted from Ref. [16])

6.6. Ultrafiltration Medium

Several theoretical [195] and experimental works [196] have demonstrated that nanosize porosity in a graphene membrane allows one element to pass through it, but does not let through other elements, thereby acting as an ultrafiltration medium. For example, tiny but precise holes can be used for desalinating sea water [197] and potentially for separating different gases [198, 199]. The desired porosity can be achieved in a number of ways, such as ion bombardment [200, 201], electron beam irradiation [202], chemical etching and surface-assisted aryl-aryl coupling of cyclohexa-m-phenylene [203, 204].

6.6.1. DNA Translocation

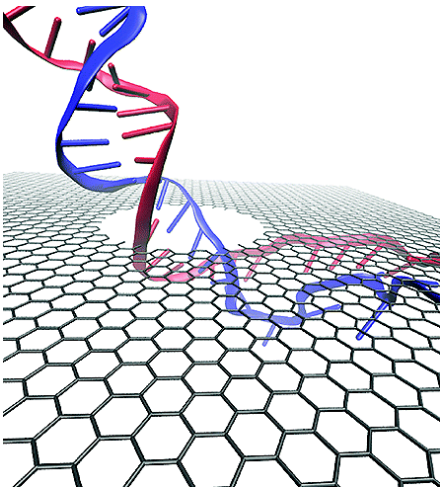

Figure 29. DNA translocation through graphene membrane (adapted from Ref. [205])

A free-standing nanoporous monolayer graphene membrane is a single atom thick (~3 Å), which is close to the stacking distance (~3.4 Å) of a DNA base pair [205]. Moreover, a graphene membrane is robust; it can withstand large membrane pressure; it is a very good electrical conductor and can be used as an electrode and simultaneously as a membrane. On the other hand, DNA has a negative charge and thus it can be pulled through the nanoporous graphene by applying an electric field. Because of these reasons, a graphene nanopore would be convenient for DNA translocation and sequencing with a single-base resolution [206]. Unlike the traditional Sanger method, graphene nanopores provide faster, reduced-cost, higher resolution DNA sequencing. The first reported DNA translocation was done by Merchant *et al.* through a 1–5 nm thick graphene membrane having 5–10 nm diameter nanopores fabricated by electron-beam [207]. Garaj *et al.* translocated DNA through a nanoporous graphene membrane of 1 nm thickness immersed in AgCl ionic solution [196].

6.6.2. Desalination

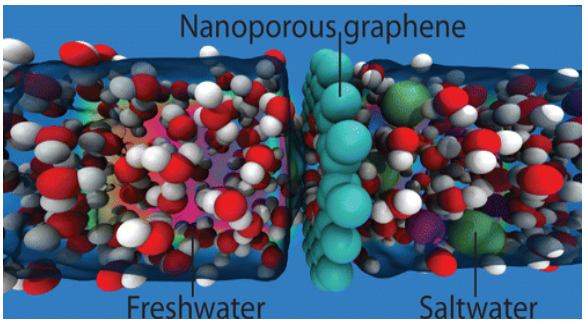

Figure 30. Schematic of desalination of seawater by nanoporous graphene (adapted from Ref. [197])

Cohen-Tanugi *et al.* [197], who predicted desalination with graphene for the first time, used an MD simulation, where a hydroxylated/hydrogeneted nanoporous graphene membrane was used, and a reverse osmosis was applied. The nonoholes let the water through and left the salt-bonded larger entity on the other side. Although graphene nanopores could be made using ion and electron bombardment [208], the steeper experimental challenge is to create cost-effective, scalable right-diameter (< 1 nm, [209]) pores for efficient desalination [210]. Unlike current polyamide-based filters, water will easily flow through graphene because of its thinness and large pressure-withstanding capability. Thus desalination through nanoporous graphene would potentially be fast, more energy efficient than any other available process in this field, and thus would be cost-effective [211].

7. Summary

In this work, we reviewed the mechanical, electromechanical, thermomechanical and related properties of graphenic material for MEMS and other membrane applications. Graphene's outstanding mechanical, electromechanical, and thermomechanical properties were instrumental in evergrowing research in fabricating graphene-based sensors and devices. Efficient dissipation of heat linked with the highest reported thermal conductivity of graphene provides a special advantage for graphene MEMS. Moreover, for fabricating graphene-based devices and ensuring their stability over long period of time, knowledge about accurate coefficient of thermal expansion (CTE) of graphene at different temperatures is mandatory. Although several transduction techniques are available, robust transduction of mechanical motion still represents a central challenge for graphene MEMS. Recently engineered piezoelectric properties of graphene [8, 16] which is comparable to those of conventional piezoelectric material, provide a promising approach for future transduction and in applications such as actuators, and energy harvesters.

Graphene's high piezoresistivity, large pressure withstanding capability, and atomic thickness are the main properties that created huge potential for graphene based pressure sensors [17, 19, 116]. The higher sensitivity, smaller dimension, transparency, flexibility of graphene-based strain sensor [18, 115, 157] are useful in fabricating touch screen, artificial electronic skin [160], and finger movement detection [157].

A major drawback of graphene resonator is the low quality factor ($Q<10^3$) at room temperature compared to state-of-the-art Q-factor ($Q\sim10^6$, [149]) of high-tensile Si_3N_4 or SiC resonator. However, the temperature reduction can significantly improve the Q of graphene resonator and

as the temperature approaches to mK range, the quality factor of graphene resonator become as high as $\sim 10^5$ [21]. The higher Young's modulus of graphene and the larger surface-to-volume ratio stemming from its atomic thickness make the graphene resonators promising for ultra-low charge, force and mass detection. The source of dissipation in graphene nanomechanical resonators is not properly explained in the literature, which is a major limitation and therefore providing a large scope for future research.

An economically viable mass production of high-quality graphene via environmentally friendly and mass-nontransferable processes is still a challenging problem. With the advent of new, innovative graphene synthesis routes, this situation is improving at a good pace. Future research is necessary for graphene growth process control, fast and efficient pre-evaluation of graphene quality and adhesion, and for integrating graphene into MEMS at wafer level. Adhesion energy between graphene and its substrate is of paramount importance for microfabrication. Whereas transfer-free graphene such as catalytic graphene has demonstrated sufficient adhesion, the next step for exfoliated or CVD graphene is to work on further improving the adhesion with the substrate because sufficient adhesion is a precondition for realizing wafer-level fabrication of graphene-based MEMS.

The extremely promising performance of graphene-based sensors and devices offers exciting possibilities for the application of graphene in MEMS. However, we can see that there is still a need to address the reproducibility problems of graphene devices in order to make their real-life application possible. Reproducibly of sensitivity, adhesion, and thermomechanical characteristics is highly desirable in MEMS and more research should be conducted to overcome the dependency of these properties on the fabrication process. Although graphene is showing an ever-increasing potential and compatibility with the mature IC technologies developed for silicon, integrating graphene into MEMS at a wafer level is still a steeper challenge.

Acknowledgments

FI is the recipient of an Australian Research Council Future Fellowship (FT120100445). Support from the AFOSR through the grant AOARD 15IOA053 is also acknowledged, as well as infrastructure support through the Australian National Fabrication Facility (ANFF).

References

[1] Novoselov K S, Geim A K, Morozov S, Jiang D, Zhang Y, Dubonos S a, Grigorieva I and Firsov A 2004 Electric field effect in atomically thin carbon films *Science* **306** 666-9

[2] The Royal Schwedish Academy of Science. Scientific Background on the Nobel Prize in Physics 2010.

[3] Fuhrer M S, Lau C N and MacDonald A H 2010 Graphene: materially better carbon *MRS Bulletin* **35** 289-95

[4] Lee C, Wei X, Kysar J W and Hone J 2008 Measurement of the elastic properties and intrinsic strength of monolayer graphene *Science* **321** 385-8

[5] Xu L, Wei N, Xu X, Fan Z and Zheng Y 2013 Defect-activated self-assembly of multilayered graphene paper: a mechanically robust architecture with high strength *Journal of Materials Chemistry A* **1** 2002-10

[6] Li Y 2016 Reversible wrinkles of monolayer graphene on a polymer substrate: toward stretchable and flexible electronics *Soft matter* **12** 3202-13

[7] Tomori H, Kanda A, Goto H, Ootuka Y, Tsukagoshi K, Moriyama S, Watanabe E and Tsuya D 2011 Introducing nonuniform strain to graphene using dielectric nanopillars *Applied physics express* **4** 075102

[8] Wang X, Tian H, Xie W, Shu Y, Mi W-T, Mohammad M A, Xie Q-Y, Yang Y, Xu J-B and Ren T-L 2015 Observation of a giant two-dimensional band-piezoelectric effect on biaxial-strained graphene *NPG Asia Materials* **7** e154

[9] Bae S, Kim H, Lee Y, Xu X, Park J-S, Zheng Y, Balakrishnan J, Lei T, Kim H R and Song Y I 2010 Roll-to-roll production of 30-inch graphene films for transparent electrodes *Nature nanotechnology* **5** 574-8

[10] Khan U, May P, O'Neill A and Coleman J N 2010 Development of stiff, strong, yet tough composites by the addition of solvent exfoliated graphene to polyurethane *Carbon* **48** 4035-41

[11] Jan R, Habib A and Gul I H 2016 Stiff, strong, yet tough free-standing dielectric films of graphene nanosheets-polyurethane nanocomposites with very high dielectric constant and loss *Electronic Materials Letters* **12** 91-9

[12] Jang H, Park Y J, Chen X, Das T, Kim M S and Ahn J H 2016 Graphene-Based Flexible and Stretchable Electronics *Advanced Materials*

[13] Lee H, Kim M, Kim I and Lee H 2016 Flexible and Stretchable Optoelectronic Devices using Silver Nanowires and Graphene *Advanced Materials*

[14] Ahmed M, Khawaja M, Notarianni M, Wang B, Goding D, Gupta B, Boeckl J J, Takshi A, Motta N and Saddow S E 2015 A thin film approach for SiC-derived graphene as an on-chip electrode for supercapacitors *Nanotechnology* **26** 434005

[15] Wang B, Ahmed M, Wood B and Iacopi F 2016 All-solid-state supercapacitors on silicon using graphene from silicon carbide *Applied Physics Letters* **108** 183903

[16] da Cunha Rodrigues G, Zelenovskiy P, Romanyuk K, Luchkin S, Kopelevich Y and Kholkin A 2015 Strong piezoelectricity in single-layer graphene deposited on SiO2 grating substrates *Nature communications* **6**

[17] Smith A D, Vaziri S, Niklaus F, Fischer A C, Sterner M, Delin A, Östling M and Lemme M C 2013 Pressure sensors based on suspended graphene membranes *Solid-State Electronics* **88** 89-94

[18] Zhao J, He C, Yang R, Shi Z, Cheng M, Yang W, Xie G, Wang D, Shi D and Zhang G 2012 Ultra-sensitive strain sensors based on piezoresistive nanographene films *Applied Physics Letters* **101** 063112

[19] Smith A, Niklaus F, Paussa A, Vaziri S, Fischer A C, Sterner M, Forsberg F, Delin A, Esseni D and Palestri P 2013 Electromechanical piezoresistive sensing in suspended graphene membranes *Nano letters* **13** 3237-42

[20] Bunch J S, Van Der Zande A M, Verbridge S S, Frank I W, Tanenbaum D M, Parpia J M, Craighead H G and McEuen P L 2007 Electromechanical resonators from graphene sheets *Science* **315** 490-3

[21] Eichler A, Moser J, Chaste J, Zdrojek M, Wilson-Rae I and Bachtold A 2011 Nonlinear damping in mechanical resonators made from carbon nanotubes and graphene *Nature nanotechnology* **6** 339-42

[22] Balandin A A, Ghosh S, Bao W, Calizo I, Teweldebrhan D, Miao F and Lau C N 2008 Superior thermal conductivity of single-layer graphene *Nano letters* **8** 902-7

[23] Seol J H, Moore A L, Shi L, Jo I and Yao Z 2011 Thermal conductivity measurement of graphene exfoliated on silicon dioxide *Journal of Heat Transfer* **133** 022403

[24] Ghosh S, Calizo I, Teweldebrhan D, Pokatilov E, Nika D, Balandin A, Bao W, Miao F and Lau C N 2008 Extremely high thermal conductivity of graphene: Prospects for thermal management applications in nanoelectronic circuits *Applied Physics Letters* **92** 151911

[25] Yoon D, Son Y-W and Cheong H 2011 Negative thermal expansion coefficient of graphene measured by Raman spectroscopy *Nano letters* **11** 3227-31

[26] Iacopi F, Brongersma S, Vandevelde B, O'Toole M, Degryse D, Travaly Y and Maex K 2004 Challenges for structural stability of ultra-low-k-based interconnects *Microelectronic engineering* **75** 54-62

[27] Li X, Cai W, An J, Kim S, Nah J, Yang D, Piner R, Velamakanni A, Jung I and Tutuc E 2009 Large-area synthesis of high-quality and uniform graphene films on copper foils *Science* **324** 1312-4

[28] Obraztsov A, Obraztsova E, Tyurnina A and Zolotukhin A 2007 Chemical vapor deposition of thin graphite films of nanometer thickness *Carbon* **45** 2017-21

[29] Novoselov K, Geim A K, Morozov S, Jiang D, Katsnelson M, Grigorieva I, Dubonos S and Firsov A 2005 Two-dimensional gas of massless Dirac fermions in graphene *nature* **438** 197-200

[30] Emtsev K V, Bostwick A, Horn K, Jobst J, Kellogg G L, Ley L, McChesney J L, Ohta T, Reshanov S A and Röhrl J 2009 Towards wafer-size graphene layers by atmospheric pressure graphitization of silicon carbide *Nature materials* **8** 203-7

[31] De Heer W A, Berger C, Wu X, First P N, Conrad E H, Li X, Li T, Sprinkle M, Hass J and Sadowski M L 2007 Epitaxial graphene *Solid State Communications* **143** 92-100

[32] Giesbers A, Bouten P, Cillessen J, van der Tempel L, Klootwijk J, Pesquera A, Centeno A, Zurutuza A, Balkenende A and van der Tempel I L 2016 Defects, a challenge for graphene in flexible electronics *Solid State Communications*

[33] Polat E O, Balci O, Kakenov N, Kocabas C and Dahiya R 2015 Synthesis of graphene on ultra-smooth copper foils for large area flexible electronics. In: *Ph. D. Research in Microelectronics and Electronics (PRIME), 2015 11th Conference on*: IEEE) pp 53-6

[34] Shao Y, El-Kady M F, Wang L J, Zhang Q, Li Y, Wang H, Mousavi M F and Kaner R B 2015 Graphene-based materials for flexible supercapacitors *Chemical Society Reviews* **44** 3639-65

[35] Petrone N, Meric I, Chari T, Shepard K L and Hone J 2015 Graphene field-effect transistors for radio-frequency flexible electronics *Electron Devices Society, IEEE Journal of the* **3** 44-8

[36] Merisalu M, Kahro T, Kozlova J, Niilisk A, Nikolajev A, Marandi M, Floren A, Alles H and Sammelselg V 2015 Graphene–polypyrrole thin hybrid corrosion resistant coatings for copper *Synthetic Metals* **200** 16-23

[37] Prasai D, Tuberquia J C, Harl R R, Jennings G K and Bolotin K I 2012 Graphene: corrosion-inhibiting coating *ACS nano* **6** 1102-8

[38] Sutter E, Albrecht P, Camino F E and Sutter P 2010 Monolayer graphene as ultimate chemical passivation layer for arbitrarily shaped metal surfaces *Carbon* **48** 4414-20

[39] Kirkland N, Schiller T, Medhekar N and Birbilis N 2012 Exploring graphene as a corrosion protection barrier *Corrosion Science* **56** 1-4

[40] Chen S, Brown L, Levendorf M, Cai W, Ju S-Y, Edgeworth J, Li X, Magnuson C W, Velamakanni A and Piner R D 2011 Oxidation resistance of graphene-coated Cu and Cu/Ni alloy *ACS nano* **5** 1321-7

[41] Capasso A, Castillo A D R, Sun H, Ansaldo A, Pellegrini V and Bonaccorso F 2015 Ink-jet printing of graphene for flexible electronics: An environmentally-friendly approach *Solid State Communications* **224** 53-63

[42] Li J, Ye F, Vaziri S, Muhammed M, Lemme M C and Östling M 2013 Efficient inkjet printing of graphene *Advanced materials* **25** 3985-92

[43] Secor E B, Prabhumirashi P L, Puntambekar K, Geier M L and Hersam M C 2013 Inkjet printing of high conductivity, flexible graphene patterns *The journal of physical chemistry letters* **4** 1347-51

[44] Finn D J, Lotya M, Cunningham G, Smith R J, McCloskey D, Donegan J F and Coleman J N 2014 Inkjet deposition of liquid-exfoliated graphene and MoS 2 nanosheets for printed device applications *Journal of Materials Chemistry C* **2** 925-32

[45] Qian W, Hao R, Zhou J, Eastman M, Manhat B A, Sun Q, Goforth A M and Jiao J 2013 Exfoliated graphene-supported Pt and Pt-based alloys as electrocatalysts for direct methanol fuel cells *Carbon* **52** 595-604

[46] Sun H, Castillo A E D R, Monaco S, Capasso A, Ansaldo A, Prato M, Dinh D A, Pellegrini V, Scrosati B and Manna L 2016 Binder-free graphene as an advanced anode for lithium batteries *Journal of Materials Chemistry A*

[47] Sun C, Li F, Ma C, Wang Y, Ren Y, Yang W, Ma Z, Li J, Chen Y and Kim Y 2014 Graphene–Co 3 O 4 nanocomposite as an efficient bifunctional catalyst for lithium–air batteries *Journal of Materials Chemistry A* **2** 7188-96

[48] Reddy A L M, Srivastava A, Gowda S R, Gullapalli H, Dubey M and Ajayan P M 2010 Synthesis of nitrogen-doped graphene films for lithium battery application *ACS nano* **4** 6337-42

[49] Ahmed M, Kishi N, Sugita R, Fukaya A, Khatri I, Liang J, Mominuzzaman S M, Soga T and Jimbo T 2013 Graphene synthesis by thermal chemical vapor deposition using solid precursor *Journal of Materials Science: Materials in Electronics* **24** 2151-5

[50] Ahmed M, Kishi N and Soga T 2015 Large scale bi-layer graphene by suppression of nucleation from a solid precursor *RSC Advances* **5** 42645-52

[51] Ahmed M, Uddin M J, Rahman M A, Kishi N and Soga T 2016 Controlled Cu Nanoparticle Growth on Wrinkle Affecting Deposition of Large Scale Graphene *Journal of Crystal Growth*

[52] Iacopi F, Ahmed M and Cunning B V 2014 Process for forming graphene layers on silicon carbide. US Patent App. 15/022,532)

[53] Cunning B V, Ahmed M, Mishra N, Kermany A R, Wood B and Iacopi F 2014 Graphitized silicon carbide microbeams: wafer-level, self-aligned graphene on silicon wafers *Nanotechnology* **25** 325301

[54] Iacopi F, Mishra N, Cunning B V, Goding D, Dimitrijev S, Brock R, Dauskardt R H, Wood B and Boeckl J 2015 A catalytic alloy approach for graphene on epitaxial SiC on silicon wafers *Journal of Materials Research* **30** 609-16

[55] Wei X, Fragneaud B, Marianetti C A and Kysar J W 2009 Nonlinear elastic behavior of graphene: Ab initio calculations to continuum description *Physical Review B* **80** 205407

[56] Liu F, Ming P and Li J 2007 Ab initio calculation of ideal strength and phonon instability of graphene under tension *Physical Review B* **76** 064120

[57] Lee J-U, Yoon D and Cheong H 2012 Estimation of Young's modulus of graphene by Raman spectroscopy *Nano letters* **12** 4444-8

[58] Ovid'ko I 2013 Mechanical properties of graphene *Rev. Adv. Mater. Sci* **34** 1-11

[59] Lee C, Wei X, Li Q, Carpick R, Kysar J W and Hone J 2009 Elastic and frictional properties of graphene *physica status solidi (b)* **246** 2562-7

[60] Ruiz-Vargas C S, Zhuang H L, Huang P Y, van der Zande A M, Garg S, McEuen P L, Muller D A, Hennig R G and Park J 2011 Softened elastic response and unzipping in chemical vapor deposition graphene membranes *Nano letters* **11** 2259-63

[61] Huang M, Pascal T A, Kim H, Goddard III W A and Greer J R 2011 Electronic− mechanical coupling in graphene from in situ nanoindentation experiments and multiscale atomistic simulations *Nano letters* **11** 1241-6

[62] Liu Y, Zhang D, Wang K, Liu Y and Shang Y 2016 A novel strain sensor based on graphene composite films with layered structure *Composites Part A: Applied Science and Manufacturing* **80** 95-103

[63] Zhang Y Y and Gu Y 2013 Mechanical properties of graphene: Effects of layer number, temperature and isotope *Computational Materials Science* **71** 197-200

[64] Subrina S, Kotchetkov D and Balandin A A 2009 Heat removal in silicon-on-insulator integrated circuits with graphene lateral heat spreaders *Electron Device Letters, IEEE* **30** 1281-3

[65] Pop E, Mann D, Wang Q, Goodson K and Dai H 2006 Thermal conductance of an individual single-wall carbon nanotube above room temperature *Nano letters* **6** 96-100

[66] Kim P, Shi L, Majumdar A and McEuen P 2001 Thermal transport measurements of individual multiwalled nanotubes *Physical review letters* **87** 215502

[67] Klemens P and Pedraza D 1994 Thermal conductivity of graphite in the basal plane *Carbon* **32** 735-41

[68] Seol J H, Jo I, Moore A L, Lindsay L, Aitken Z H, Pettes M T, Li X, Yao Z, Huang R and Broido D 2010 Two-dimensional phonon transport in supported graphene *Science* **328** 213-6

[69] Chen S, Wu Q, Mishra C, Kang J, Zhang H, Cho K, Cai W, Balandin A A and Ruoff R S 2012 Thermal conductivity of isotopically modified graphene *Nature materials* **11** 203-7

[70] Los J, Zakharchenko K, Katsnelson M and Fasolino A 2015 Melting temperature of graphene *Physical Review B* **91** 045415

[71] Zakharchenko K, Fasolino A, Los J and Katsnelson M 2011 Melting of graphene: from two to one dimension *Journal of Physics: Condensed Matter* **23** 202202

[72] Gao W and Huang R 2014 Thermomechanics of monolayer graphene: Rippling, thermal expansion and elasticity *Journal of the Mechanics and Physics of Solids* **66** 42-58

[73] Mounet N and Marzari N 2005 First-principles determination of the structural, vibrational and thermodynamic properties of diamond, graphite, and derivatives *Physical Review B* **71** 205214

[74] Singh V, Sengupta S, Solanki H S, Dhall R, Allain A, Dhara S, Pant P and Deshmukh M M 2010 Probing thermal expansion of graphene and modal dispersion at low-temperature using graphene nanoelectromechanical systems resonators *Nanotechnology* **21** 165204

[75] Jiang J-W, Wang J-S and Li B 2009 Thermal expansion in single-walled carbon nanotubes and graphene: Nonequilibrium Green's function approach *Physical Review B* **80** 205429

[76] Bao W, Miao F, Chen Z, Zhang H, Jang W, Dames C and Lau C N 2009 Controlled ripple texturing of suspended graphene and ultrathin graphite membranes *Nature nanotechnology* **4** 562-6

[77] Steward E, Cook B and Kellett E 1960 Dependence on temperature of the interlayer spacing in carbons of different graphitic perfection

[78] Kirilenko D, Dideykin A and Van Tendeloo G 2011 Measuring the corrugation amplitude of suspended and supported graphene *Physical Review B* **84** 235417

[79] Li Q, Lee C, Carpick R W and Hone J 2010 Substrate effect on thickness-dependent friction on graphene *physica status solidi (b)* **247** 2909-14

[80] Ko J-H, Kwon S, Byun I-S, Choi J S, Park B H, Kim Y-H and Park J Y 2013 Nanotribological properties of fluorinated, hydrogenated, and oxidized graphenes *Tribology Letters* **50** 137-44

[81] Kwon S, Ko J-H, Jeon K-J, Kim Y-H and Park J Y 2012 Enhanced nanoscale friction on fluorinated graphene *Nano letters* **12** 6043-8

[82] Kim K-S, Lee H-J, Lee C, Lee S-K, Jang H, Ahn J-H, Kim J-H and Lee H-J 2011 Chemical vapor deposition-grown graphene: the thinnest solid lubricant *ACS nano* **5** 5107-14

[83] Lee H, Lee N, Seo Y, Eom J and Lee S 2009 Comparison of frictional forces on graphene and graphite *Nanotechnology* **20** 325701

[84] Choi J S, Kim J-S, Byun I-S, Lee D H, Lee M J, Park B H, Lee C, Yoon D, Cheong H and Lee K H 2011 Friction anisotropy–driven domain imaging on exfoliated monolayer graphene *Science* **333** 607-10

[85] Szlufarska I, Chandross M and Carpick R W 2008 Recent advances in single-asperity nanotribology *Journal of Physics D: Applied Physics* **41** 123001

[86] Penkov O, Kim H-J, Kim H-J and Kim D-E 2014 Tribology of graphene: a review *International journal of precision engineering and manufacturing* **15** 577-85

[87] Carpick R W, Ogletree D and Salmeron M 1997 Lateral stiffness: a new nanomechanical measurement for the determination of shear strengths with friction force microscopy *Applied Physics Letters* **70** 1548-50

[88] Carpick R W and Salmeron M 1997 Scratching the surface: fundamental investigations of tribology with atomic force microscopy *Chemical Reviews* **97** 1163-94

[89] Lee C, Li Q, Kalb W, Liu X-Z, Berger H, Carpick R W and Hone J 2010 Frictional characteristics of atomically thin sheets *Science* **328** 76-80

[90] Wählisch F, Hoth J, Held C, Seyller T and Bennewitz R 2013 Friction and atomic-layer-scale wear of graphitic lubricants on SiC (0001) in dry sliding *Wear* **300** 78-81

[91] Filleter T, McChesney J L, Bostwick A, Rotenberg E, Emtsev K, Seyller T, Horn K and Bennewitz R 2009 Friction and dissipation in epitaxial graphene films *Physical review letters* **102** 086102

[92] Cho D-H, Wang L, Kim J-S, Lee G-H, Kim E S, Lee S, Lee S Y, Hone J and Lee C 2013 Effect of surface morphology on friction of graphene on various substrates *Nanoscale* **5** 3063-9

[93] Filleter T and Bennewitz R 2010 Structural and frictional properties of graphene films on SiC (0001) studied by atomic force microscopy *Physical Review B* **81** 155412

[94] Rastei M, Heinrich B and Gallani J 2013 Puckering Stick-Slip Friction Induced by a Sliding Nanoscale Contact *Physical review letters* **111** 084301

[95] Lin L-Y, Kim D-E, Kim W-K and Jun S-C 2011 Friction and wear characteristics of multi-layer graphene films investigated by atomic force microscopy *Surface and Coatings Technology* **205** 4864-9

[96] Mechanical Reliability of Microelectronic Interfaces.

[97] Boztug C, Sánchez-Pérez J R, Cavallo F, Lagally M G and Paiella R 2014 Strained-germanium nanostructures for infrared photonics *ACS nano* **8** 3136-51

[98] Koenig S P, Boddeti N G, Dunn M L and Bunch J S 2011 Ultrastrong adhesion of graphene membranes *Nature nanotechnology* **6** 543-6

[99] Boddeti N G, Koenig S P, Long R, Xiao J, Bunch J S and Dunn M L 2013 Mechanics of adhered, pressurized graphene blisters *Journal of Applied Mechanics* **80** 040909

[100] Cao Z, Wang P, Gao W, Tao L, Suk J, Ruoff R, Akinwande D, Huang R and Liechti K 2014 A blister test for interfacial adhesion of large-scale transferred graphene *Carbon* **69** 390-400

[101] Zong Z, Chen C-L, Dokmeci M R and Wan K-t 2010 Direct measurement of graphene adhesion on silicon surface by intercalation of nanoparticles *Journal of Applied Physics* **107** 026104

[102] Das S, Lahiri D, Lee D-Y, Agarwal A and Choi W 2013 Measurements of the adhesion energy of graphene to metallic substrates *Carbon* **59** 121-9

[103] Yoon T, Shin W C, Kim T Y, Mun J H, Kim T-S and Cho B J 2012 Direct measurement of adhesion energy of monolayer graphene as-grown on copper and its application to renewable transfer process *Nano letters* **12** 1448-52

[104] Wells G, Hopf T, Vassilevski K, Escobedo-Cousin E, Wright N, Horsfall A, Goss J, O'Neill A and Hunt M 2014 Determination of the adhesion energy of graphene on SiC (0001) via measurement of pleat defects *Applied Physics Letters* **105** 193109

[105] Ferralis N, Maboudian R and Carraro C 2008 Evidence of structural strain in epitaxial graphene layers on 6H-SiC (0001) *Physical review letters* **101** 156801

[106] Riedl C, Coletti C, Iwasaki T, Zakharov A and Starke U 2009 Quasi-free-standing epitaxial graphene on SiC obtained by hydrogen intercalation *Physical review letters* **103** 246804

[107] Ni Z H, Yu T, Lu Y H, Wang Y Y, Feng Y P and Shen Z X 2008 Uniaxial strain on graphene: Raman spectroscopy study and band-gap opening *ACS nano* **2** 2301-5

[108] Bunch J S and Dunn M L 2012 Adhesion mechanics of graphene membranes *Solid State Communications* **152** 1359-64

[109] KHATIBI E 2011 Piezoresistivity of graphene

[110] Kanda Y 1991 Piezoresistance effect of silicon *Sensors and Actuators A: Physical* **28** 83-91

[111] Yang W, He C, Zhang L, Wang Y, Shi Z, Cheng M, Xie G, Wang D, Yang R and Shi D 2012 Growth, characterization, and properties of nanographene *Small* **8** 1429-35

[112] Hosseinzadegan H, Todd C, Lal A, Pandey M, Levendorf M and Park J 2012 Graphene has ultra high piezoresistive gauge factor. In: *Micro Electro Mechanical Systems (MEMS), 2012 IEEE 25th International Conference on*: IEEE) pp 611-4

[113] Lee Y, Bae S, Jang H, Jang S, Zhu S-E, Sim S H, Song Y I, Hong B H and Ahn J-H 2010 Wafer-scale synthesis and transfer of graphene films *Nano letters* **10** 490-3

[114] Wang Y, Yang R, Shi Z, Zhang L, Shi D, Wang E and Zhang G 2011 Super-elastic graphene ripples for flexible strain sensors *ACS nano* **5** 3645-50

[115] Kim Y-J, Cha J Y, Ham H, Huh H, So D-S and Kang I 2011 Preparation of piezoresistive nano smart hybrid material based on graphene *Current Applied Physics* **11** S350-S2

[116] Zhu S-E, Ghatkesar M K, Zhang C and Janssen G 2013 Graphene based piezoresistive pressure sensor *Applied Physics Letters* **102** 161904

[117] Christel L and Petersen K 1993 A catheter pressure sensor with side vent using multiple silicon fusion bonding. In: *7th International Conference on Solid− State Sensors and Actuators (Transducers' 93), Yokohama, Japan*, pp 7-10

[118] Melvås P 2002 Ultraminiaturized Pressure Sensor for Catheter Based Applications

[119] Fung C K, Zhang M Q, Chan R H and Li W J 2005 A PMMA-based micro pressure sensor chip using carbon nanotubes as sensing elements. In: *Micro Electro Mechanical Systems, 2005. MEMS 2005. 18th IEEE International Conference on*: IEEE) pp 251-4

[120] Bunch J S, Verbridge S S, Alden J S, van der Zande A M, Parpia J M, Craighead H G and McEuen P L 2008 Impermeable atomic membranes from graphene sheets *Nano letters* **8** 2458-62

[121] Zhang Y 2006 In situ fatigue crack detection using piezoelectric paint sensor *Journal of Intelligent Material Systems and Structures* **17** 843-52

[122] Kijanka P, Packo P, Staszewski W J and di Scalea F L 2016 Actuation stress modelling of piezoceramic transducers under variable temperature field *Journal of Intelligent Material Systems and Structures* **27** 337-49

[123] Ong M T and Reed E J 2012 Engineered piezoelectricity in graphene *ACS nano* **6** 1387-94

[124] Chandratre S and Sharma P 2012 Coaxing graphene to be piezoelectric *Applied Physics Letters* **100** 023114

[125] Xu Y, Chen C, Deshpande V V, DiRenno F A, Gondarenko A, Heinz D B, Liu S, Kim P and Hone J 2010 Radio frequency electrical transduction of graphene mechanical resonators *Applied Physics Letters* **97** 243111

[126] Chen C, Rosenblatt S, Bolotin K I, Kalb W, Kim P, Kymissis I, Stormer H L, Heinz T F and Hone J 2009 Performance of monolayer graphene nanomechanical resonators with electrical readout *Nature nanotechnology* **4** 861-7

[127] Matsui K, Inaba A, Oshidari Y, Takei Y, Takahashi H, Takahata T, Kometani R, Matsumoto K and Shimoyama I 2014 Mechanical properties of few layer graphene cantilever. In: *Micro Electro Mechanical Systems (MEMS), 2014 IEEE 27th International Conference on*: IEEE) pp 1087-90

[128] Berinskii I, Indeitsev D, Morozov N, Skubov D Y and Shtukin L 2015 Differential graphene resonator as a mass detector *Mechanics of Solids* **50** 127-34

[129] Barton R A, Ilic B, van der Zande A M, Whitney W S, McEuen P L, Parpia J M and Craighead H G 2011 High, size-dependent quality factor in an array of graphene mechanical resonators *Nano letters* **11** 1232-6

[130] Wong C, Annamalai M, Wang Z and Palaniapan M 2010 Characterization of nanomechanical graphene drum structures *Journal of Micromechanics and Microengineering* **20** 115029

[131] Patel R N, Mathew J P, Borah A and Deshmukh M M 2016 Low tension graphene drums for electromechanical pressure sensing *2D Materials* **3** 011003

[132] Barton R A, Storch I R, Adiga V P, Sakakibara R, Cipriany B R, Ilic B, Wang S P, Ong P, McEuen P L and Parpia J M 2012 Photothermal self-oscillation and laser cooling of graphene optomechanical systems *Nano letters* **12** 4681-6

[133] Stemme G 1991 Resonant silicon sensors *Journal of Micromechanics and Microengineering* **1** 113

[134] Naik A, Hanay M, Hiebert W, Feng X and Roukes M 2009 Towards single-molecule nanomechanical mass spectrometry *Nature nanotechnology* **4** 445-50

[135] Barton R A, Parpia J and Craighead H G 2011 Fabrication and performance of graphene nanoelectromechanical systems *Journal of Vacuum Science & Technology B* **29** 050801

[136] Oshidari Y, Hatakeyama T, Kometani R, Warisawa S i and Ishihara S 2012 High quality factor graphene resonator fabrication using resist shrinkage-induced strain *Applied Physics Express* **5** 117201

[137] Kermany A R, Bennett J S, Valenzuela V M, Bowen W P and Iacopi F 2016 Potential of epitaxial silicon carbide microbeam resonators for chemical sensing *physica status solidi (a)*

[138] Chen C and Hone J 2013 Graphene nanoelectromechanical systems *Proceedings of the IEEE* **101** 1766-79

[139] Sazonova V, Yaish Y, Üstünel H, Roundy D, Arias T A and McEuen P L 2004 A tunable carbon nanotube electromechanical oscillator *Nature* **431** 284-7

[140] Gouttenoire V, Barois T, Perisanu S, Leclercq J L, Purcell S T, Vincent P and Ayari A 2010 Digital and FM Demodulation of a Doubly Clamped Single-Walled Carbon-Nanotube Oscillator: Towards a Nanotube Cell Phone *Small* **6** 1060-5

[141] Lee S, Chen C, Deshpande V V, Lee G-H, Lee I, Lekas M, Gondarenko A, Yu Y-J, Shepard K and Kim P 2013 Electrically integrated SU-8 clamped graphene drum resonators for strain engineering *Applied Physics Letters* **102** 153101

[142] Chen C, Deshpande V V, Koshino M, Lee S, Gondarenko A, MacDonald A H, Kim P and Hone J 2016 Modulation of mechanical resonance by chemical potential oscillation in graphene *Nature Physics* **12** 240-4

[143] Chen C, Lee S, Deshpande V V, Lee G-H, Lekas M, Shepard K and Hone J 2013 Graphene mechanical oscillators with tunable frequency *Nature nanotechnology* **8** 923-7

[144] Zande A M v d, Barton R A, Alden J S, Ruiz-Vargas C S, Whitney W S, Pham P H, Park J, Parpia J M, Craighead H G and McEuen P L 2010 Large-scale arrays of single-layer graphene resonators *Nano letters* **10** 4869-73

[145] Garcia-Sanchez D, van der Zande A M, Paulo A S, Lassagne B, McEuen P L and Bachtold A 2008 Imaging mechanical vibrations in suspended graphene sheets *Nano letters* **8** 1399-403

[146] Kim S Y and Park H S 2009 The importance of edge effects on the intrinsic loss mechanisms of graphene nanoresonators *Nano letters* **9** 969-74

[147] Jiang J-W and Wang J-S 2012 Why edge effects are important on the intrinsic loss mechanisms of graphene nanoresonators *Journal of Applied Physics* **111** 054314

[148] Miao T, Yeom S, Wang P, Standley B and Bockrath M 2014 Graphene nanoelectromechanical systems as stochastic-frequency oscillators *Nano letters* **14** 2982-7

[149] Kermany A R, Brawley G, Mishra N, Sheridan E, Bowen W P and Iacopi F 2014 Microresonators with Q-factors over a million from highly stressed epitaxial silicon carbide on silicon *Applied Physics Letters* **104** 081901

[150] Takamura M, Okamoto H, Furukawa K, Yamaguchi H and Hibino H 2014 Energy dissipation in edged and edgeless graphene mechanical resonators *Journal of Applied Physics* **116** 064304

[151] Verbridge S S, Craighead H G and Parpia J M 2008 A megahertz nanomechanical resonator with room temperature quality factor over a million *Applied Physics Letters* **92** 13112-

[152] Robinson J T, Zalalutdinov M, Baldwin J W, Snow E S, Wei Z, Sheehan P and Houston B H 2008 Wafer-scale reduced graphene oxide films for nanomechanical devices *Nano letters* **8** 3441-5

[153] Zalalutdinov M K, Robinson J T, Junkermeier C E, Culbertson J C, Reinecke T L, Stine R, Sheehan P E, Houston B H and Snow E S 2012 Engineering graphene mechanical systems *Nano letters* **12** 4212-8

[154] Adhikari S and Chowdhury R 2012 Zeptogram sensing from gigahertz vibration: Graphene based nanosensor *Physica E: Low-dimensional Systems and Nanostructures* **44** 1528-34

[155] De Alba R, Massel F, Storch I, Abhilash T, Hui A, McEuen P, Craighead H and Parpia J 2016 Tunable phonon cavity coupling in graphene membranes *arXiv preprint arXiv:1604.04605*

[156] Mathew J P, Patel R N, Borah A, Vijay R and Deshmukh M M 2016 Dynamical strong coupling and parametric amplification of mechanical modes of graphene drums *Nature nanotechnology*

[157] Yan C, Wang J, Kang W, Cui M, Wang X, Foo C Y, Chee K J and Lee P S 2014 Highly stretchable piezoresistive graphene–nanocellulose nanopaper for strain sensors *Advanced materials* **26** 2022-7

[158] Ren T-L, Tian H, Xie D and Yang Y 2012 Flexible graphite-on-paper piezoresistive sensors *Sensors* **12** 6685-94

[159] Kälvesten E, Smith L, Tenerz L and Stemme G 1998 The first surface micromachined pressure sensor for cardiovascular pressure measurements. In: *Micro Electro Mechanical*

Systems, 1998. MEMS 98. Proceedings., The Eleventh Annual International Workshop on: IEEE) pp 574-9

[160] Zhao J, Wang G, Yang R, Lu X, Cheng M, He C, Xie G, Meng J, Shi D and Zhang G 2015 Tunable Piezoresistivity of Nanographene Films for Strain Sensing *ACS nano* **9** 1622-9

[161] Yamada T, Hayamizu Y, Yamamoto Y, Yomogida Y, Izadi-Najafabadi A, Futaba D N and Hata K 2011 A stretchable carbon nanotube strain sensor for human-motion detection *Nature nanotechnology* **6** 296-301

[162] AliáMohammad M 2015 A flexible, transparent and ultrathin single-layer graphene earphone *RSC Advances* **5** 17366-71

[163] Suk J W, Kirk K, Hao Y, Hall N A and Ruoff R S 2012 Thermoacoustic sound generation from monolayer graphene for transparent and flexible sound sources *Advanced Materials* **24** 6342-7

[164] Tian H, Xie D, Yang Y, Ren T-L, Wang Y-F, Zhou C-J, Peng P-G, Wang L-G and Liu L-T 2012 Single-layer graphene sound-emitting devices: experiments and modeling *Nanoscale* **4** 2272-7

[165] Tian H, Ren T-L, Xie D, Wang Y-F, Zhou C-J, Feng T-T, Fu D, Yang Y, Peng P-G and Wang L-G 2011 Graphene-on-paper sound source devices *ACS nano* **5** 4878-85

[166] Fei W, Zhou J and Guo W 2015 Low-voltage Driven Graphene Foam Thermoacoustic Speaker *Small* **11** 2252-6

[167] Tian H, Li C, Mohammad M A, Cui Y-L, Mi W-T, Yang Y, Xie D and Ren T-L 2014 Graphene earphones: Entertainment for both humans and animals *ACS nano* **8** 5883-90

[168] Zhou Q and Zettl A 2013 Electrostatic graphene loudspeaker *Applied Physics Letters* **102** 223109

[169] Nayak P K, Hsu C-J, Wang S-C, Sung J C and Huang J-L 2013 Graphene coated Ni films: A protective coating *Thin Solid Films* **529** 312-6

[170] Pop E, Varshney V and Roy A K 2012 Thermal properties of graphene: Fundamentals and applications *MRS bulletin* **37** 1273-81

[171] Nair R, Blake P, Grigorenko A, Novoselov K, Booth T, Stauber T, Peres N and Geim A 2008 Fine structure constant defines visual transparency of graphene *Science* **320** 1308-

[172] Schriver M, Regan W, Gannett W J, Zaniewski A M, Crommie M F and Zettl A 2013 Graphene as a long-term metal oxidation barrier: worse than nothing *ACS nano* **7** 5763-8

[173] Nilsson L, Andersen M, Balog R, Lægsgaard E, Hofmann P, Besenbacher F, Hammer B, Stensgaard I and Hornekær L 2012 Graphene coatings: probing the limits of the one atom thick protection layer *ACS nano* **6** 10258-66

[174] Huh J-H, Kim S H, Chu J H, Kim S Y, Kim J H and Kwon S-Y 2014 Enhancement of seawater corrosion resistance in copper using acetone-derived graphene coating *Nanoscale* **6** 4379-86

[175] Jiang D-e, Sumpter B G and Dai S 2007 Unique chemical reactivity of a graphene nanoribbon's zigzag edge *The Journal of chemical physics* **126** 134701

[176] Jin J, Wang X and Song M 2011 Graphene-based nanostructured hybrid materials for conductive and superhydrophobic functional coatings *Journal of nanoscience and nanotechnology* **11** 7715-22

[177] Li N, Liu L and Yang F 2014 Highly conductive graphene/PANi-phytic acid modified cathodic filter membrane and its antifouling property in EMBR in neutral conditions *Desalination* **338** 10-6

[178] Anandan S, Narasinga Rao T, Sathish M, Rangappa D, Honma I and Miyauchi M 2012 Superhydrophilic graphene-loaded TiO2 thin film for self-cleaning applications *ACS applied materials & interfaces* **5** 207-12

[179] Wang X, Song L, Yang H, Lu H and Hu Y 2011 Synergistic effect of graphene on antidripping and fire resistance of intumescent flame retardant poly (butylene succinate) composites *Industrial & Engineering Chemistry Research* **50** 5376-83

[180] Shi Y, Qian X, Zhou K, Tang Q, Jiang S, Wang B, Wang B, Yu B, Hu Y and Yuen R K 2013 CuO/graphene nanohybrids: preparation and enhancement on thermal stability and

smoke suppression of polypropylene *Industrial & Engineering Chemistry Research* **52** 13654-60

[181] Jiang S-D, Bai Z-M, Tang G, Hu Y and Song L 2014 Synthesis of ZnS decorated graphene sheets for reducing fire hazards of epoxy composites *Industrial & Engineering Chemistry Research* **53** 6708-17

[182] Berman D, Erdemir A and Sumant A V 2013 Few layer graphene to reduce wear and friction on sliding steel surfaces *Carbon* **54** 454-9

[183] Won M-S, Penkov O V and Kim D-E 2013 Durability and degradation mechanism of graphene coatings deposited on Cu substrates under dry contact sliding *Carbon* **54** 472-81

[184] Berman D, Erdemir A and Sumant A V 2013 Reduced wear and friction enabled by graphene layers on sliding steel surfaces in dry nitrogen *Carbon* **59** 167-75

[185] Marsden A J, Phillips M and Wilson N R 2013 Friction force microscopy: a simple technique for identifying graphene on rough substrates and mapping the orientation of graphene grains on copper *Nanotechnology* **24** 255704

[186] Berman D, Deshmukh S A, Sankaranarayanan S K, Erdemir A and Sumant A V 2015 Macroscale superlubricity enabled by graphene nanoscroll formation *Science* **348** 1118-22

[187] Bolotin K I, Sikes K, Jiang Z, Klima M, Fudenberg G, Hone J, Kim P and Stormer H 2008 Ultrahigh electron mobility in suspended graphene *Solid State Communications* **146** 351-5

[188] Lee H-L, Yang Y-C and Chang W-J 2013 Mass detection using a graphene-based nanomechanical resonator *Japanese Journal of Applied Physics* **52** 025101

[189] Sone H, Fujinuma Y and Hosaka S 2004 Picogram mass sensor using resonance frequency shift of cantilever *Japanese Journal of Applied Physics* **43** 3648

[190] Abadal G, Davis Z J, Helbo B, Borrise X, Ruiz R, Boisen A, Campabadal F, Esteve J, Figueras E and Perez-Murano F 2001 Electromechanical model of a resonating nano-

cantilever-based sensor for high-resolution and high-sensitivity mass detection *Nanotechnology* **12** 100

[191] Ekinci K, Yang Y and Roukes M 2004 Ultimate limits to inertial mass sensing based upon nanoelectromechanical systems *Journal of applied physics* **95** 2682-9

[192] Lassagne B, Garcia-Sanchez D, Aguasca A and Bachtold A 2008 Ultrasensitive mass sensing with a nanotube electromechanical resonator *Nano letters* **8** 3735-8

[193] Chaste J, Eichler A, Moser J, Ceballos G, Rurali R and Bachtold A 2012 A nanomechanical mass sensor with yoctogram resolution *Nature nanotechnology* **7** 301-4

[194] Ekinci K, Huang X and Roukes M 2004 Ultrasensitive nanoelectromechanical mass detection *Applied Physics Letters* **84** 4469-71

[195] Sun C, Boutilier M S, Au H, Poesio P, Bai B, Karnik R and Hadjiconstantinou N G 2014 Mechanisms of molecular permeation through nanoporous graphene membranes *Langmuir* **30** 675-82

[196] Garaj S, Hubbard W, Reina A, Kong J, Branton D and Golovchenko J 2010 Graphene as a subnanometre trans-electrode membrane *Nature* **467** 190-3

[197] Cohen-Tanugi D and Grossman J C 2012 Water desalination across nanoporous graphene *Nano letters* **12** 3602-8

[198] Jiang D-e, Cooper V R and Dai S 2009 Porous graphene as the ultimate membrane for gas separation *Nano letters* **9** 4019-24

[199] Hauser A W and Schwerdtfeger P 2012 Nanoporous graphene membranes for efficient 3He/4He separation *The Journal of Physical Chemistry Letters* **3** 209-13

[200] O'Hern S C, Boutilier M S, Idrobo J-C, Song Y, Kong J, Laoui T, Atieh M and Karnik R 2014 Selective ionic transport through tunable subnanometer pores in single-layer graphene membranes *Nano letters* **14** 1234-41

[201] Bell D C, Lemme M C, Stern L A, Williams J R and Marcus C M 2009 Precision cutting and patterning of graphene with helium ions *Nanotechnology* **20** 455301

[202] Fischbein M D and Drndić M 2008 Electron beam nanosculpting of suspended graphene sheets *Applied Physics Letters* **93** 113107

[203] Xu P, Yang J, Wang K, Zhou Z and Shen P 2012 Porous graphene: properties, preparation, and potential applications *Chinese Science Bulletin* **57** 2948-55

[204] Wen B, Sun C and Bai B 2015 Inhibition effect of a non-permeating component on gas permeability of nanoporous graphene membranes *Physical Chemistry Chemical Physics* **17** 23619-26

[205] Sathe C, Zou X, Leburton J-P and Schulten K 2011 Computational investigation of DNA detection using graphene nanopores *ACS nano* **5** 8842-51

[206] Postma H W C 2010 Rapid sequencing of individual DNA molecules in graphene nanogaps *Nano letters* **10** 420-5

[207] Merchant C A, Healy K, Wanunu M, Ray V, Peterman N, Bartel J, Fischbein M D, Venta K, Luo Z and Johnson A C 2010 DNA translocation through graphene nanopores *Nano letters* **10** 2915-21

[208] Russo C J and Golovchenko J 2012 Atom-by-atom nucleation and growth of graphene nanopores *Proceedings of the National Academy of Sciences* **109** 5953-7

[209] Suk M E and Aluru N 2010 Water transport through ultrathin graphene *The Journal of Physical Chemistry Letters* **1** 1590-4

[210] Wang E N and Karnik R 2012 Water desalination: Graphene cleans up water *Nature nanotechnology* **7** 552-4

[211] Cohen-Tanugi D and Grossman J C 2015 Nanoporous graphene as a reverse osmosis membrane: Recent insights from theory and simulation *Desalination* **366** 59-70